Stem Cell Reports
Article

ISSCR

OPEN ACCESS

Histone 2B-GFP Label-Retaining Prostate Luminal Cells Possess Progenitor Cell Properties and Are Intrinsically Resistant to Castration

Dingxiao Zhang,[1,2,*] Collene Jeter,[2] Shuai Gong,[2,4] Amanda Tracz,[1] Yue Lu,[2] Jianjun Shen,[2] and Dean G. Tang[1,2,3,*]

[1]Department of Pharmacology and Therapeutics, Roswell Park Cancer Institute, Elm & Carlton Streets, Buffalo, NY 14263, USA
[2]Department of Epigenetics and Molecular Carcinogenesis, University of Texas MD Anderson Cancer Center, Smithville, TX 78957, USA
[3]Cancer Stem Cell Institute, Research Center for Translational Medicine, East Hospital, Tongji University, Shanghai 200120, PR China
[4]Present address: The First Affiliated Hospital of Zhengzhou University, Zhengzhou 450052, PR China
*Correspondence: dingxiao.zhang@roswellpark.org (D.Z.), dean.tang@roswellpark.org (D.G.T.)
https://doi.org/10.1016/j.stemcr.2017.11.016

SUMMARY

The existence of slow-cycling luminal cells in the prostate has been suggested, but their identity and functional properties remain unknown. Using a bigenic mouse model to earmark, isolate, and characterize the quiescent stem-like cells, we identify a label-retaining cell (LRC) population in the luminal cell layer as luminal progenitors. Molecular and biological characterizations show that these luminal LRCs are significantly enriched in the mouse proximal prostate, exhibit relative dormancy, display bipotency in both *in vitro* and *in vivo* assays, and express a stem/progenitor gene signature with resemblance to aggressive prostate cancer. Importantly, these LRCs, compared with bulk luminal cells, maintain a lower level of androgen receptor (AR) expression and are less androgen dependent and also castration resistant *in vivo*. Finally, analysis of phenotypic markers reveals heterogeneity within the luminal progenitor cell pool. Our study establishes luminal LRCs as progenitors that may serve as a cellular origin for castration-resistant prostate cancer.

INTRODUCTION

The prostatic gland contains basal and luminal epithelial cells, together with rare neuroendocrine cells. Luminal cells express cytokeratin (CK) 18 and androgen receptor (AR) and are androgen dependent, whereas basal cells express CK5 and stem cell (SC) transcription factor p63 and are androgen independent (Shen and Abate-Shen, 2010). Developmentally, the murine prostate originates from an ancestral $p63^{+}AR^{-}$ basal SC population (Pignon et al., 2013). Studies using prostate regeneration assays demonstrate that multipotent SCs capable of differentiating into all prostatic cell types are localized in the basal layer (Kwon and Xin, 2014). Therefore, basal cells are thought to represent the main pool of prostate stem cells (PSCs) (Wang et al., 2013). However, lineage-tracing studies indicate that basal cells rarely generate luminal cells during adult tissue homeostasis but display plasticity under the inductive influence of embryonic urogenital mesenchyme (UGM) cells in tissue regeneration assays, acquiring facultative stem/progenitor cell properties and generating luminal cells (Choi et al., 2012; Wang et al., 2013). Consequently, both cell layers in adult murine prostate are self-sustained by lineage-restricted stem/progenitor cells (Choi et al., 2012), although more primitive SCs reside in the basal layer (Ousset et al., 2012). An *in vitro* organoid assay recently identified a small fraction (<1%) of luminal cells functionally defined as multipotent luminal progenitors in that they were able to generate organoids containing both basal and luminal cells (Karthaus et al., 2014). Beyond homeostasis, several rare luminal progenitor populations have been reported in regressed mouse prostates, including castration-resistant NKX3.1-expressing (CARN) (Wang et al., 2009), $SCA\text{-}1^{+}$ (Kwon et al., 2016), and castration-resistant BMI1-expressing (CARB) (Yoo et al., 2016) cells. The precise relationship between these luminal progenitor cell populations remains unclear.

The prostate has been a model for studying tissue SCs, because it undergoes atrophy upon castration and regeneration upon re-administration of androgen, and this regression-regeneration cycle can be repeated multiple times. Somatic SCs are generally dormant and this cardinal slow-cycling feature is frequently utilized to identify putative SCs by labels that become diluted as a result of cell division (Tang, 2012). Studies have shown that label-retaining cells (LRCs) in many organs are enriched for SCs (dos Santos et al., 2013; Foudi et al., 2009; Szotek et al., 2008; Tsujimura et al., 2002; Tumbar et al., 2004; Wang et al., 2012). Previously, 5-bromodeoxyuridine (BrdU) was employed to perform pulse-chase experiments to identify candidate SCs. In the prostate, a long-term chased $BrdU^{+}$ cell population, encompassing both basal and luminal cells, which resides in the proximal region of mouse prostatic ducts and exhibits attributes of epithelial SCs was proposed as PSCs (Tsujimura et al., 2002). Whether these dormant cells truly represent SCs has not been answered mainly due to the technical infeasibility of purifying out live $BrdU^{+}$ cells for functional studies. More recently, cell surface markers coupled with fluorescence-activated cell sorting (FACS) have been used to dissect the subsets

of cells within a bulk population. These assays depend on known SC markers, and, notably, the majority of widely used markers (e.g., SCA-1, CD49f) preferentially identify prostate basal stem-like cells (Lawson et al., 2007; Lukacs et al., 2010a; Stoyanova et al., 2012; Xin et al., 2005), leaving the luminal cell compartment under-studied. Lineage-tracing technology has greatly enhanced our understanding of SC development; however, lineage-tracing studies only suggest that a certain cell population harbors SCs, but could not pinpoint which precise cell(s) within the population is SC (Rycaj and Tang, 2015).

In this study, we employed a bigenic mouse model to identify, isolate, and characterize the stem-like properties and gene expression profiles of quiescent LRCs from mouse prostates expressing a tunable H2B-GFP driven by the promoter of a luminal lineage-preferential gene *probasin* (Suraneni et al., 2010). Biological and molecular studies show that long-term chased luminal LRCs are inherently resistant to castration and can generate organoids *in vitro* and prostatic glands *in vivo*. Notably, the LRC-derived organoids and prostatic glands contain both basal and luminal cells, suggesting the bipotency of LRCs. RNA sequencing (RNA-seq) analysis of this rare population reveals a progenitor-like transcriptome that resembles therapy-resistant prostate cancer (PCa). Analysis of a spectrum of phenotypic markers previously linked to epithelial cell stemness reveals heterogeneity in luminal progenitor populations. Collectively, our study augments our understanding of prostate luminal progenitors and provides valuable insights into their potential roles in prostate development and, possibly, cancer initiation and progression.

RESULTS

Establishing a Bigenic Mouse Model to Label Slow-Cycling Cells in Prostatic Epithelium

To study the dormant cell population in the luminal cell compartment, we adopted a Tet-Off system similar to that described previously (Tumbar et al., 2004) by engineering a Pb-tetVP16 transgenic line to express tetracycline repressor-VP16 controlled by *probasin* (*Pbsn*)-based *ARR2Pb* promoter (Zhang et al., 2000; Figure S1A). By crossing the Pb-tetVP16 mice with the tetracycline-responsive element-regulated mCMV/H2B-GFP reporter mice (Tumbar et al., 2004), we generated the bigenic mice, Pb-tetVP16-GFP, in which GFP expression is ultimately driven by *Pbsn* promoter (Figures S1A and S1B). In this way, without doxycycline (DOX) administration (pulse), the prostate tissues would be largely GFP$^+$. Upon DOX administration (chase), the prostate will gradually lose the GFP signal due to cell division, while infrequently cycling and dormant cells would retain GFP for an extended period of time (Figure S1A). Indeed, the whole prostate or microdissected prostate branches from the unchased young adult (6 weeks) animals were green, and GFP intensity dropped accordingly at different intervals of chase (Figure 1A). These data demonstrate the successful establishment of a bigenic mouse model to fluorescently label slow-cycling cells in the prostatic epithelium.

H2B-GFP Primarily Labels Prostate Luminal Cells

We assessed the expression and distribution of GFP$^+$ cells in the adult prostate glands. Consistent with the reported activity of endogenous *Pbsn* promoter (Zhang et al., 2000), GFP signal was higher in ventral prostate (VP) and dorsal and lateral prostate (DLP) than that in anterior prostate (AP) (Figure 1B). As a marker of differentiation and androgen action in the mouse prostate, Pbsn is primarily expressed in the luminal epithelial cells. Double immunofluorescence (IF) staining of CK5 or CK8 and GFP indicated that, as expected, GFP$^+$ cells were mainly localized to the luminal compartment in unchased prostates (Figure 1C). Consistent with the varying gross GFP intensity in different prostate lobes (Figure 1B), the frequency of GFP$^+$ cells was much higher in VP (79.4%) and DLP (79.4%) than that in AP (43.8%) (Figures 1C and S1C; Table S1). We also observed some GFP$^+$CK5$^+$ double-positive cells (Figure 1C, solid arrows) and non-epithelial GFP$^+$ cells in the stromal compartment (Figure S1C), suggesting that the *Pbsn* promoter is also active in a small subset of basal and stromal cells, as reported previously (Valdez et al., 2012; Wang et al., 2006). Interestingly, during the course of this work and consistent with a prior study (Wang et al., 2014a), we frequently noticed many GFP$^+$ luminal cells in the lumen (Figure 1C, dashed arrows), implying that luminal cells have a faster turnover than basal cells (see below).

Kinetics of H2B-GFP LRCs in Basal and Luminal Cell Layers

To characterize optimal chase time and kinetic changes in GFP$^+$ cells, we quantified the percentage of GFP$^+$ cells at different time points after chase according to their lineage identity (Figures 1C–1E and 2A). We started chasing the male mice at 6–8 weeks when the prostate is generally well developed. The initial luminal cell-labeling efficacy was 79.4%, 79.4%, and 43.8% for VP, DLP, and AP, respectively (Table S1). As expected, upon chase, prostatic cells gradually lost GFP signal (Figures 2B and S2A). By 9-week chase, the percentage of GFP$^+$ luminal cells dropped from ~80% to <20% in VP, and by 14-week chase and after, GFP$^+$ cells were rarely seen (Figures 2C and S2A). After a 12-week chase, the luminal GFP$^+$ cells remained at 2%–6% in different lobes (Figure 2C). Consequently, we referred to the GFP$^+$ cells that persisted for at least a 12-week chase as LRCs. This time point is in line with studies in other

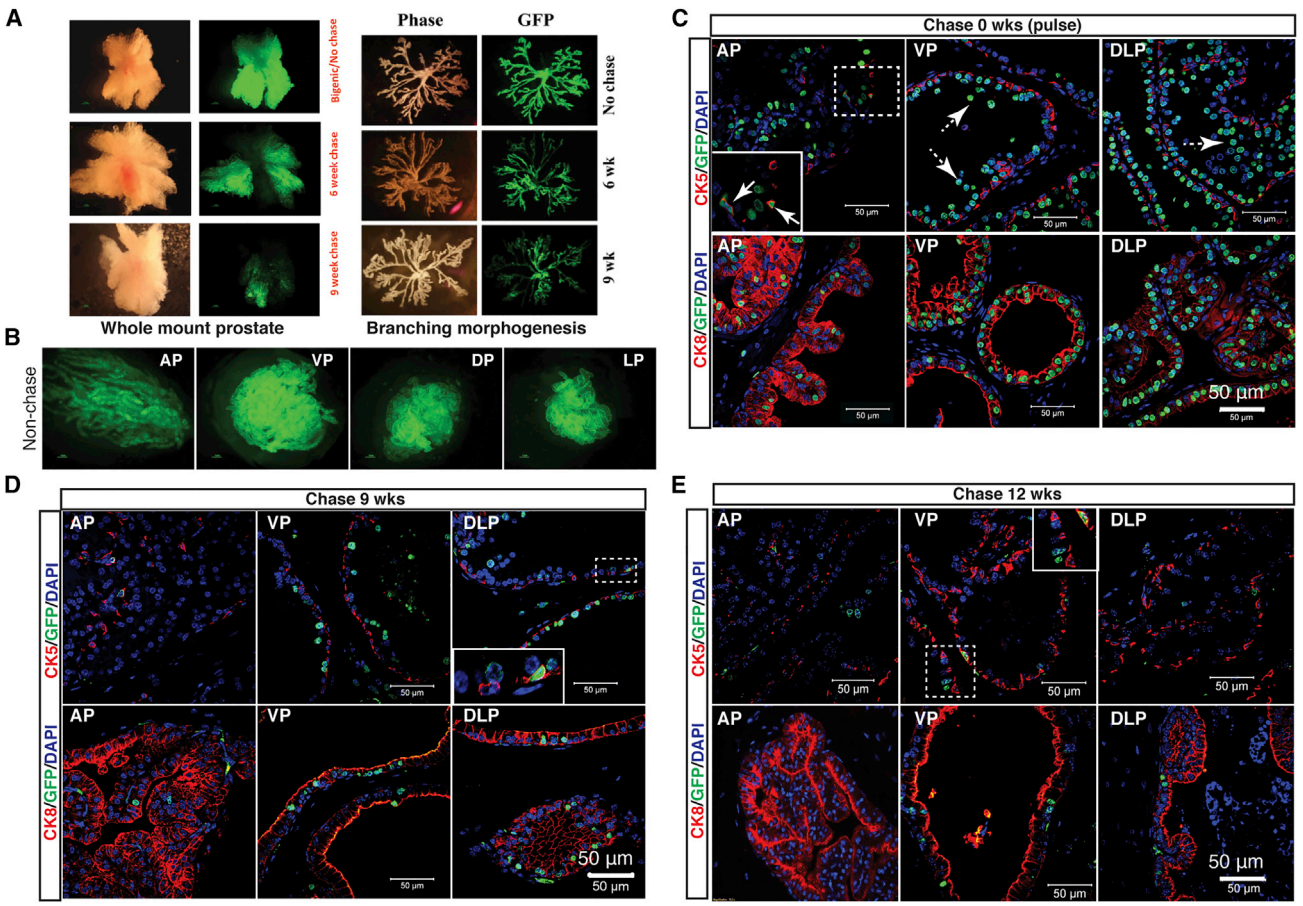

Figure 1. Identification of H2B-GFP LRCs

(A) Loss of GFP signals in DOX-chased prostates. Shown are gross GFP images in whole-mount prostates (left) and microdissected prostate branches (right) isolated from bigenic mice chased for 0 weeks (no chase), 6 weeks, and 9 weeks.

(B) Gross GFP images in different lobes of prostates dissected from unchased adult Pb-tetVP16-GFP bigenic mice.

(C–E) Double IF of CK5 or CK8 and GFP in different prostate lobes harvested from bigenic mice chased (on DOX diet) for 0 weeks (C), 9 weeks (D), and 12 weeks (E). Arrows and dashed arrows in (C) (top) indicate $CK5^{+}GFP^{+}$ basal cells and luminal cells shed into the lumen, respectively. AP, VP, DP, and LP refer to anterior, ventral, dorsal, and lateral prostate lobes, respectively. Dashed boxed regions are enlarged (solid boxes). Scale bars, 50 μm.

See also Figure S1.

organs using similar H2B-GFP mouse models (dos Santos et al., 2013; Szotek et al., 2008; Wang et al., 2012). Our model also labeled a small subset of $CK5^{+}$ basal cells, with 2%–8% GFP^{+} cells in unchased lobes and 1%–3% GFP^{+} cells after a 12-week chase (Figure 2D; Table S1). Interestingly, compared with the relatively flat curve of basal GFP^{+} cell kinetics, luminal GFP^{+} cells decreased much faster as a function of chase (Figures 2C and 2D). IF analysis revealed $Ki\text{-}67^{+}$ cells exclusively in luminal layer in all lobes (Figure 2E). Furthermore, we frequently and exclusively observed symmetrically dividing GFP^{+} cells in the luminal layer (Figure 2F). These observations validated faster proliferation and loss of GFP signal in luminal cells compared with basal cells. Quantitatively, unchased young adult bigenic mice displayed a small percentage of prostatic GFP^{+} cells that co-expressed the proliferation marker Ki-67 (4.03%, 0.42%, and 1.80% for AP, VP, and DLP, respectively); in contrast, after a 12-week chase no GFP^{+} cells were stained positive for Ki-67 (Figures 2G and S2B), confirming the quiescence of LRCs.

Luminal LRCs Are Enriched in the Proximal Prostatic Ducts and Mark Progenitors Capable of Regenerating Prostate Glands *In Vivo*

We next performed *in vitro* and *in vivo* SC-related assays, first in bulk GFP^{+} LRCs. The lineage-negative (Lin^{-}) GFP^{+} cells freshly purified from the prostates chased for 12 weeks (Figure S3A) displayed higher capacity to form 2D colonies

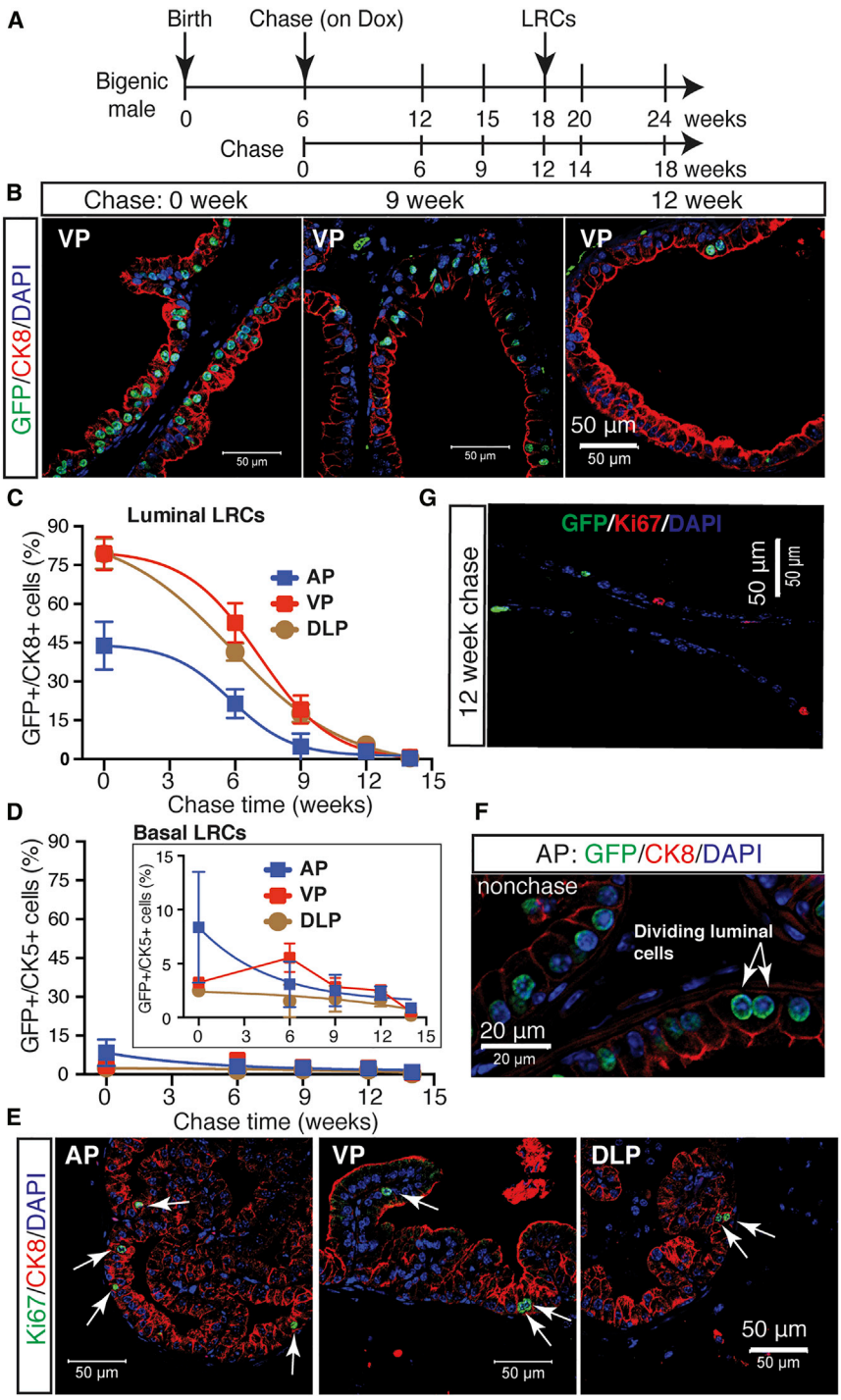

Figure 2. Dynamics and Characterization of LRCs

(A) Scheme for tracking the dynamics of prostatic GFP$^+$ cells in hormonally intact mice, in which we started chasing the bigenic animals at 6 weeks of age and analyzed the prostate tissues at different time points post chase.

(B) IF images of CK8 and GFP in the VP isolated from bigenic mice chased for different time intervals.

(C and D) Quantification of GFP$^+$ cells in luminal (C) and basal (D) cell populations as a function of chase time. At each time point, two to four mice were examined, and data are shown as the mean ± SE.

(E) IF staining of Ki67 and CK8 in different prostate lobes in wild-type adult mice. Arrows indicate Ki67$^+$CK8$^+$ cells.

(F) IF of GFP and CK8 in the AP of unchased adult bigenic mice showing symmetrical division of luminal cells.

(G) IF staining of Ki67 and GFP in the VP of bigenic mice chased for 12 weeks.

See also Figure S2 and Table S1.

and 3D spheres with larger size (Figures 3A–3C) than matched GFP$^-$ cells. *In vivo* tissue regeneration assays demonstrated that both GFP$^+$ and GFP$^-$ cells could readily regenerate prostate glandular structures with secretions in the lumen (Figure 3D). The origin of the recombinants was verified by GFP signal and staining (Figures 3D and S3B). It is worth noting that, after a 12-week chase, the LRCs were composed of both luminal and basal cells (ratio = 2:1; Table S1). As basal cells represent the main PSC pool, it is expected that GFP$^-$ population, which contained the majority of both luminal and basal cells, would also efficiently regenerate prostate tissues *in vivo*. Regardless, our

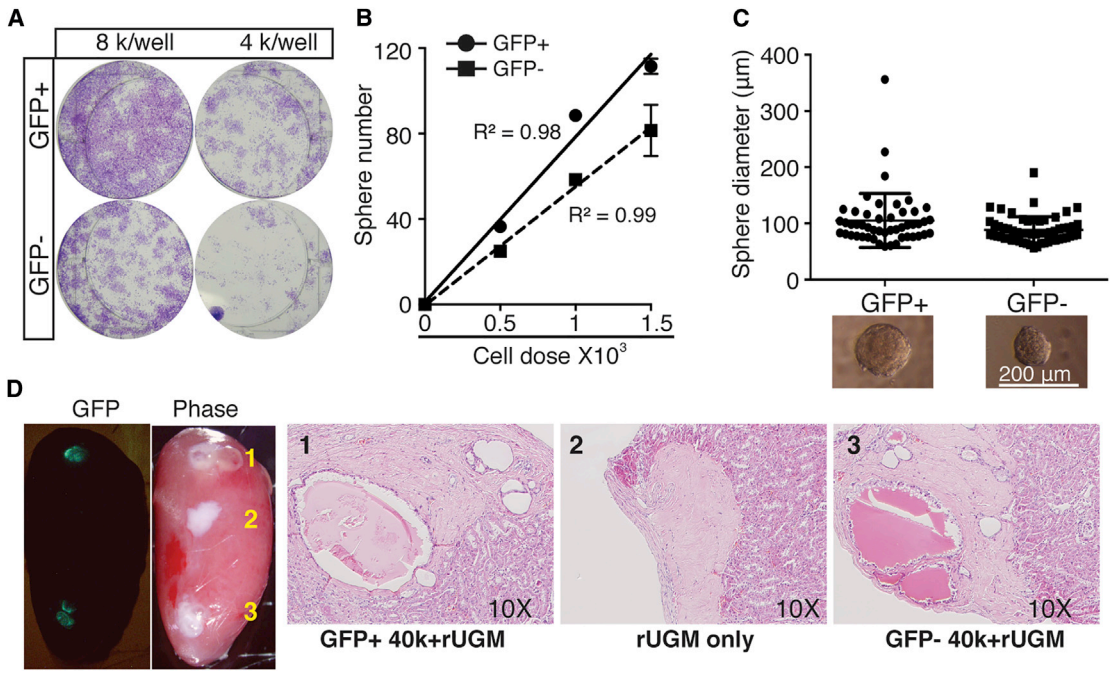

Figure 3. The LRC Population Harbors Tissue Regeneration Ability *In Vivo*

Freshly purified lineage-depleted (Lin^-) prostatic LRCs (i.e., GFP^+ cells from 12-week-chased bigenic mice) exhibit higher stem/progenitor activities than matched non-LRCs (i.e., GFP^- cells). Shown are colony formation (A), limiting-dilution sphere (B), sphere size measurement (C), and *in vivo* prostate tissue regeneration (D) assays. In (D), 1, 2, and 3 indicate the three representative recombinants. Results shown for each panel were representative data of at least two to three independent experiments showing consistent results. For (B) and (C), data are shown as the mean ± SD derived from technical replicates. See also Figure S3.

data indicate that the long-term chased LRC population harbors stem/progenitor cells with tissue regeneration ability *in vivo*.

To "zoom in" on the biological differences between luminal and basal LRCs, we purified GFP^+ cells from the two cell compartments using marker staining and FACS (Valdez et al., 2012) to identify basal ($SCA\text{-}1^+CD49f^{hi}$), luminal ($SCA\text{-}1^-CD49f^{lo}$), and stromal ($SCA\text{-}1^+CD49f^{-/lo}$) cells (Figure S4A). Since the *Pbsn* promoter is active in only a small subset of basal cells (Valdez et al., 2012; Wang et al., 2006), we considered our Pb-tetVP16-GFP bigenic model non-optimal to characterize basal SCs. In support, basal LRCs exhibited limited advantages over basal non-LRCs in SC-related assays, exhibiting slightly increased 2D clonal capacity and nearly equivalent sphere-forming cell frequency (Figures S4B and S4C), although GFP^+ basal cells did form larger 3D spheres than GFP^- basal cells (Figure S4D). Overall, these results could be explained by low labeling efficiency in the basal cell layer and high SC activity of stochastic basal cells. Therefore, for the remainder of this study we focused on luminal LRCs.

Since our initial luminal cell-labeling efficacy was ~80% for VP and DLP, we first tested whether luminal progenitor cell activity was equally distributed between the labeled and unlabeled (~20%) luminal populations in unchased adult animals. Both 2D clonal (Figure S4E) and 3D organoid (Figure S4F) assays revealed similar activities in unchased luminal (L)-GFP^+ and L-GFP^- cells, validating the suitability of our model in comparing stem/progenitor cell activities in chased L-GFP^+ and L-GFP^- cells. Freshly purified luminal LRCs from 12-week-chased prostates exhibited significantly higher clonal and organoid-forming (Figures 4A and 4B) capacities than matched luminal GFP^- cells. Importantly, luminal GFP^+ cells formed large hollow organoids, whereas only a limited number of luminal GFP^- cells formed small compact spheres (Figure 4C). Importantly, luminal LRC-derived organoids had a glandular structure reminiscent of normal prostate, with $p63^+$ and $CK5^+$ basal cells mainly residing in the peripheral layer (Figure S4G). This result is in line with recent findings that only multipotent luminal progenitors can form organoids *in vitro* (Karthaus et al., 2014). When we mixed L-GFP^+ or L-GFP^- cells (4.5×10^3) with mouse UGM and implanted subcutaneously into NOD-SCID-IL2Rγ^{null} (NSG) mice, only L-GFP^+ cells generated prostatic glandular structures with overt secretions in the lumen (Figure 4D), whereas even higher numbers of luminal GFP^- cells (up to 18×10^3) failed to

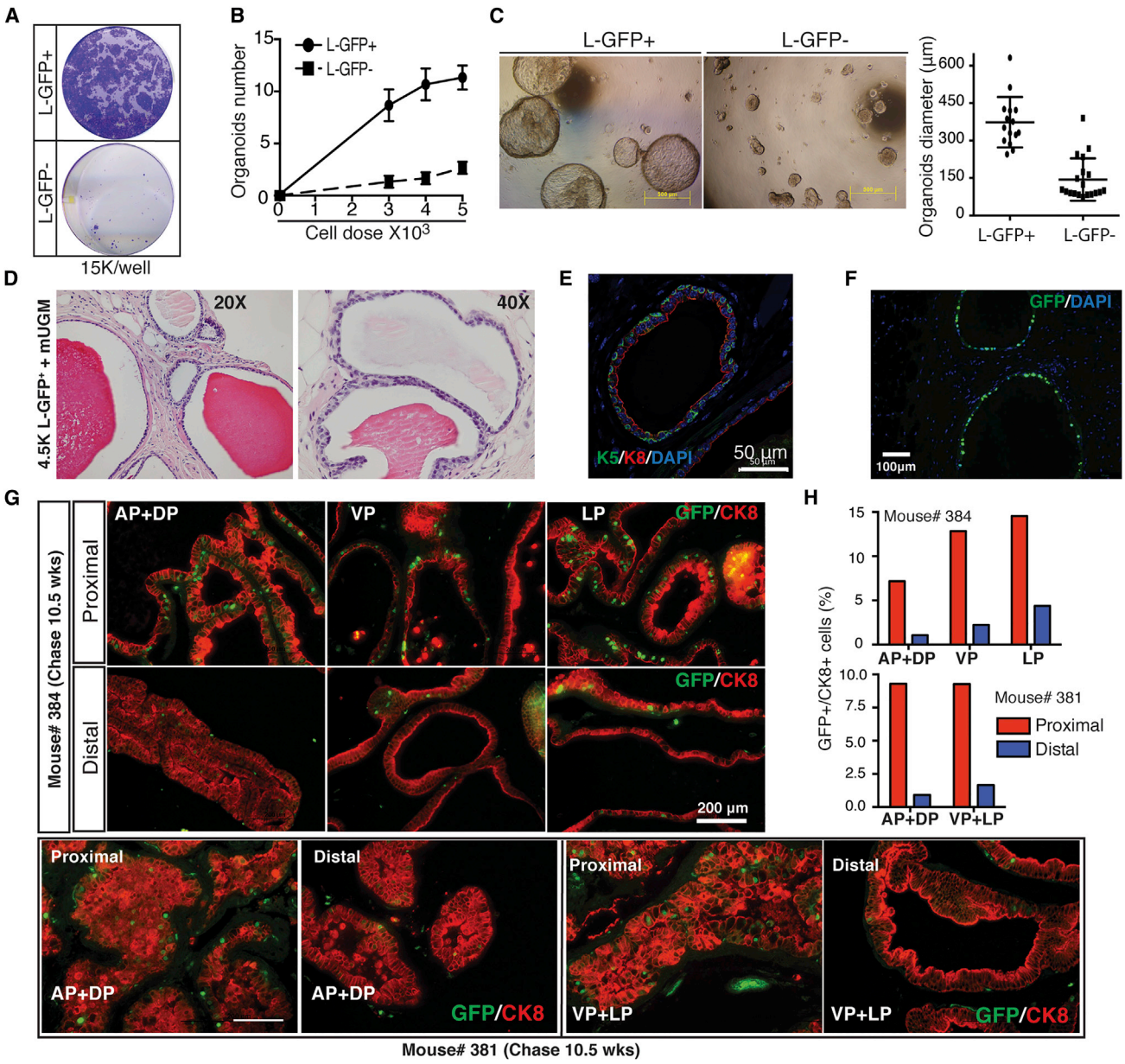

Figure 4. Luminal LRCs Mark Progenitors Capable of Regenerating Prostate Glands *In Vivo*

(A–C) Freshly purified Lin$^-$ luminal GFP$^+$ LRCs exhibit stem/progenitor activities. Shown are higher colony- (A) and organoid- (B) forming capabilities and larger sphere sizes (C) in L-GFP$^+$ compared with L-GFP$^-$ cells. For (B) and (C), data are shown as the mean ± SD derived from technical replicates.

(D–F) Only luminal GFP$^+$, but not GFP$^-$ cells, are capable of regenerating prostate tissues *in vivo*. Shown are H&E staining (D) and IF of CK5 and CK8 (E), and GFP (F) in prostate glands regenerated *in vivo* from sorted luminal GFP$^+$ cells co-injected with mouse UGM.

(G and H) Enrichment of luminal LRCs in the proximal mouse prostate. Different prostate lobes dissected from bigenic mice at 10.5 weeks of DOX chase were divided longitudinally into two portions (distal and proximal) and subjected to IF of GFP and CK8. Shown are representative images (G) and quantification data (H) from two different mice. Results shown (A)–(F) are representative data of at least two to three independent experiments showing consistent results. For (G) and (H), two bigenic mice were analyzed and data represent the means from cell number counting of five to eight random high-magnification (×20) images of each indicated category.

See also Figure S4 and Table S1.

give rise to prostatic tissue (not shown). These LRC-regenerated glands were normal-appearing with a layer of CK8$^+$ luminal cells lining the lumen and a discontinuous layer of CK5$^+$ basal cells encapsulating the structure (Figure 4E). The identity of injected cells and the LRC origin of recombinants were verified by GFP staining (Figure 4F), and the level of GFP was still detectable after several rounds of cell proliferation during prostate regeneration (not shown). These results together indicate that luminal LRCs mark luminal progenitors with bilineage differentiation capacity *in vitro* and *in vivo*.

Previous studies using a BrdU label-retention strategy suggested that putative PSCs (including both basal and luminal cells) are slow cycling and enriched in the proximal region of the prostate (Tsujimura et al., 2002). We sought to examine whether our luminal LRCs are also enriched in the proximal prostate. Each prostate lobe from mice chased for 10.5 weeks was dissected longitudinally into two portions, representing the distal and proximal prostatic ducts. IF analysis of GFP and CK8 indicated that the GFP$^+$CK8$^+$ luminal LRCs were significantly enriched in the proximal prostatic ducts adjacent to the urethra (Figures 4G and 4H).

Interestingly, when we examined the mRNA and protein level of PBSN in the pelvic urogenital sinus (UGS) of newborn and 1-week-old male mice, we observed that the *Pbsn* mRNA and PBSN protein were minimally expressed in newborn (d1) UGS but readily detectable in 1-week-old UGS (Figures S4H–S4J), suggesting that *Pbsn* is expressed early on in urogenital tissues and *Pbsn* promoter activity is not necessarily active only in mature fully differentiated luminal cells. Indeed, we detected GFP$^+$ cells co-expressing CK8 and relatively high levels of PBSN protein in pelvic UGS of 1-week-old bigenic mice (Figure S4K). These results indicate that our LRC labeling system is also suitable in marking luminal progenitor cells at early developmental stages.

Luminal LRCs Display a Luminal Progenitor Gene Expression Signature

We next sought to determine the molecular features of L-GFP$^+$ progenitors prepared from bigenic mice chased for 12 weeks. By performing genome-wide RNA-seq analysis using rRNA-depleted total RNAs (Figure 5A), we obtained an average of ~77 million reads per sample with an average mapping rate of 93% to the reference mouse genome (UCSC version mm10; Figure S5A). MA plot indicated appropriate normalization of our RNA-seq data (Figure S5B). Gene set enrichment analysis (GSEA) of RNA-seq transcriptome revealed exclusive enrichment in L-GFP$^+$ (over L-GFP$^-$) cells of gene signatures related to luminal epithelial progenitors and SCs (Figure 5B, plots 1–4). Significantly, a recently reported signature of an AR-deleted luminal cell population with a stem-like phenotype in the mouse prostate (Xie et al., 2017) was significantly enriched in our luminal LRCs (Figure 5B, plot 5). Furthermore, we recently developed an *in vitro* 2D culture system that allows enrichment of luminal progenitors from primary human prostate tissues (Zhang et al., 2017). The gene signature of this cultured-enriched human luminal progenitors (WIT-L) was also enriched in luminal LRCs (Figure 5B, plot 3). In contrast, and, as expected, signatures associated with non-progenitor cells (luminal progenitor_down), AR signaling and steroid/androgen hormone metabolism were only enriched in L-GFP$^-$ cells (Figure S5C). It has been suggested that luminal progenitors are less dependent on AR signaling (Agarwal et al., 2015; Kwon et al., 2014). Consistent with an enrichment of AR/androgen signaling in L-GFP$^-$ cells (Figure S5C) and with AR$^-$ luminal cell signature (Xie et al., 2017) in L-GFP$^+$ cells (Figure 5B, plot 5), *Ar* mRNA expression was decreased in L-GFP$^+$ cells (Figure 5C). IF analysis of GFP and AR using titrated anti-AR antibody dilutions revealed significant heterogeneity of AR expression within luminal cell population and indicated that ~37% ± 1.6% of GFP$^+$ luminal cells expressed low AR protein (Figures 5D and S5D). Interestingly, CK19, a marker for luminal transit amplifying cells (Hudson et al., 2001; Korsten et al., 2009; Wang et al., 2001), and CD24a, a cell surface marker frequently used to enrich mammary luminal progenitors (dos Santos et al., 2013; Rodilla et al., 2015), were dramatically increased in L-GFP$^+$ cells (Figure 5C). Intriguingly, we observed higher levels of *Pbsn* in L-GFP$^+$ versus L-GFP$^-$ cells (Figure 5C), perhaps indicative of the luminal nature of LRCs and also due to LRC identification by virtue of *Pbsn* promoter activities. Real-time qPCR analysis in two independently sorted biological samples confirmed slightly reduced *Ar* mRNA levels in L-GFP$^+$ cells and also validated the differentially expressed patterns of about a dozen genes in L-GFP$^+$ versus L-GFP$^-$ cells (Figure S5E; data not shown). Intriguingly, L-GFP$^+$ cells, compared with L-GFP$^-$ cells, expressed higher levels of luminal markers (*Nkx3.1, Krt8*, and *Krt18*) but lower levels of basal genes (*Trp63* and *Krt5*) (Figure S5E).

To further dissect the transcriptomic profiles in L-GFP$^+$ cells (Table S2), we performed the pathway/network enrichment analysis by Ingenuity Pathway Analysis and DAVID gene ontology annotation. The two approaches generated similar results and revealed neurogenesis, SC and development, inflammation/immunity, and cell adhesion being the top gene categories overrepresented in L-GFP$^+$ cells (Figures 5E and S5F). Interestingly, we have recently shown that normal human prostate basal/SCs (Zhang et al., 2016b) and PSA$^{-/lo}$ prostate cancer SCs (Qin et al., 2012) also preferentially express many neurogenesis-related genes. Further GSEA corroborated that,

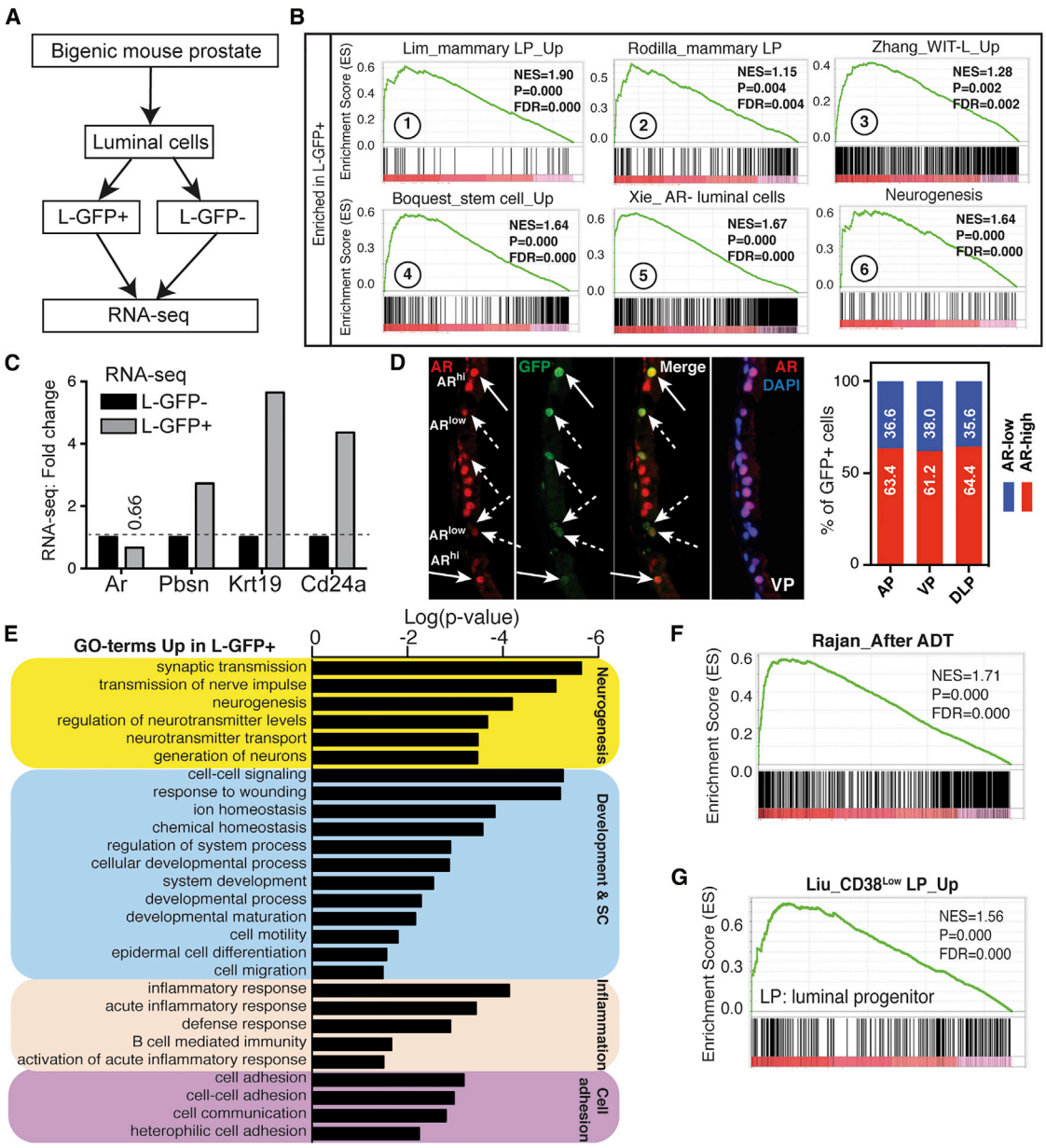

Figure 5. Luminal LRCs Display a Luminal Progenitor Gene Signature Associated with CRPC

(A) Scheme of RNA-seq experiments using freshly purified L-GFP$^+$ and L-GFP$^-$ cells from bigenic mice chased for 12 weeks.

(B) Representative GSEA results in luminal GFP$^+$ cells.

(C) Differential expression of the indicated genes in RNA-seq in L-GFP$^+$ versus L-GFP$^-$ cells.

(D) IF of GFP and AR in 12-week-chased animals. Shown are representative images (left) and quantification data (right; a total of 41, 71, and 73 GFP$^+$ cells for AP, VP, and DLP, respectively, were counted from four to six random high-magnification (×20) images of each lobe). In (D), solid arrows point to GFP$^+$/AR^{hi} cells and dashed arrows to GFP$^+$/AR^{low} cells.

(E) Functional annotation by DAVID of genes preferentially upregulated in luminal GFP$^+$ cells.

(F and G) GSEA results for the enrichment of indicated gene signatures in luminal GFP$^+$ cells.

See also Figure S5 and Table S1.

compared with L-GFP$^-$ cells, the slow-cycling L-GFP$^+$ cells were highly enriched in gene networks involved in neural/neuronal development and functions (Figures 5B, plot 6, and S5G). Surprisingly, we observed no obvious enrichment of cell-cycle-related pathways in L-GFP$^+$ cells, and a survey of key cell-cycle regulators revealed a generally

decreased expression of positive cell-cycle genes, while cell-cycle-negative regulators remained unchanged (Figure S5H). These results implicate potential involvement of other mechanisms (e.g., transforming growth factor β signaling [Salm et al., 2005]) in driving the quiescence of LRCs.

Neurogenesis and Inflammation Gene Signatures Link the Gene Expression Profile in Luminal LRCs to Aggressive and Castration-Resistant PCa

Our recent studies (Zhang et al., 2017) linked the gene expression profile in WIT-L human prostate luminal progenitors to aggressive subtypes of PCa such as CRPC (castration-resistant PCa) and neuroendocrine PCa. Further, attenuated AR activity and androgen deprivation therapy (ADT) promote a stem-like cell phenotype in PCa (Schroeder et al., 2014) and inflammation has been shown to expand a progenitor-like luminal cell pool (Liu et al., 2016) and decrease AR signaling in human prostatic luminal cells (Zhang et al., 2016a). These discussions prompted us to determine whether the gene expression profile in luminal LRCs could be linked to clinical features of PCa. GSEA revealed a significant enrichment of gene signatures of WIT-L human luminal progenitors in L-GFP$^+$ cells (Figure 5B, plot 3), suggesting that the luminal LRC gene profile may associate with aggressive PCa phenotypes. In support, gene signatures in patient CRPC after failure of ADT were enriched in L-GFP$^+$ cells (Figures 5F and S5I). These latter observations may suggest a global progenitor-like gene expression profile in human CRPC.

Of interest, a gene signature of mouse prostate tumors originated from basal cells (Wang et al., 2013) was modestly but significantly enriched in L-GFP$^+$ cells (Figure S5J), suggesting that prostate tumors with a basal cell origin may be maintained by luminal progenitor-like cells, consistent with an earlier study (Stoyanova et al., 2013). Importantly, a recently reported gene signature of a human CD38^{low} prostatic luminal progenitor population was dramatically enriched in our L-GFP$^+$ cells (Figure 5G). Of note, the CD38^{low} human luminal progenitors are tightly associated with inflammation in PCa, express an inflammatory signature with reduced AR and androgen signaling, and associate with disease progression and poor outcome (Liu et al., 2016). Thus, our mouse luminal LRCs share molecular features with human prostatic luminal progenitors.

Luminal LRCs Resist Castration *In Vivo*

The cellular origin(s) of castration resistance is a central question in PCa research and a long-standing hypothesis is that stem/progenitor cells may preferentially survive ADT. Consequently, we evaluated the *in vivo* castration sensitivity of luminal LRCs. To first assess whether our model could label luminal cells intrinsically resistant to castration, we castrated the unchased Pb-tetVP16-GFP male mice at 6–8 weeks and then started DOX chase and examined the abundance of GFP$^+$ cells in prostate lobes at different time points after castration. Numerous GFP$^+$ cells (8.0%, 29.3%, and 20.1% for AP, VP, and DLP, respectively) were observed at even 12 weeks after castration (Figure S6A), suggesting that our model marks a proportion of luminal cells that are intrinsically castration resistant in physiological conditions. We next sought to evaluate whether long-term chased LRCs resist castration. We castrated 10- to 12-week-chased bigenic male mice and analyzed prostates 1–4 weeks later (Figures 6A–6D). As short as 1 week after castration, seminal vesicles and prostate glands shrank significantly (Figures 6A and 6C), suggesting successful androgen ablation. In all experimental settings, the frequency of luminal LRCs (GFP$^+$CK8$^+$) dramatically increased post castration, indicating that GFP$^+$ cells possessed intrinsic survival advantages over GFP$^-$ cells (Figures 6A–6D). For example, in uncastrated bigenic mice chased for 14 weeks, very few GFP$^+$ cells were seen (Figure S2A); in contrast, abundant GFP$^+$ cells remained in the prostates of mice castrated at 10–12 weeks and harvested at 13- to 14-week chase (Figures 6B–6D). We also examined whether LRCs resist apoptosis after castration by co-IF analysis of GFP and cleaved caspase-3 in the prostates castrated at 12- to 13-week chase and harvested at 3 days, 1 week, and 2 weeks post castration (Figure S6B). Apoptosis in mouse prostatic luminal cells generally peaks at 3–4 days after castration and persists, at declining levels, in the following 1–3 weeks (Kato et al., 2013). Notably, we did not detect any GFP$^+$ LRC cells expressing cleaved caspase-3 in all three experimental settings (Figure S6B), suggesting that castration-induced apoptosis in LRCs is a rare event. To further determine whether the increased number of GFP$^+$ LRCs was due to proliferation besides resistance to apoptosis, we performed co-IF of Ki67 and GFP in the above experimental settings. A small number of Ki67$^+$ epithelial cells were observed in regressed prostates (e.g., 1-week [Figure S6C] or 2-weeks [Figure S6D] post castration), but no GFP$^+$ Ki67$^+$ LRCs were found (Figure S6D), consistent with the dormancy of LRCs. These results collectively demonstrate that luminal LRCs preferentially survive androgen deprivation.

Phenotypic Analysis of LRCs Reveals Heterogeneity in Luminal Progenitor Cells

Several surface markers have been reported for mouse mammary luminal progenitors, including SCA-1 (or LY6A), CD133, CD117, CD14, CD24 (Shehata et al., 2012), NOTCH3 (Lafkas et al., 2013), and NOTCH1 (Rodilla et al., 2015). Other than SCA-1 (Burger et al., 2005), similar phenotypic studies in the mouse prostate under physiological (i.e., homeostatic) conditions are generally lacking.

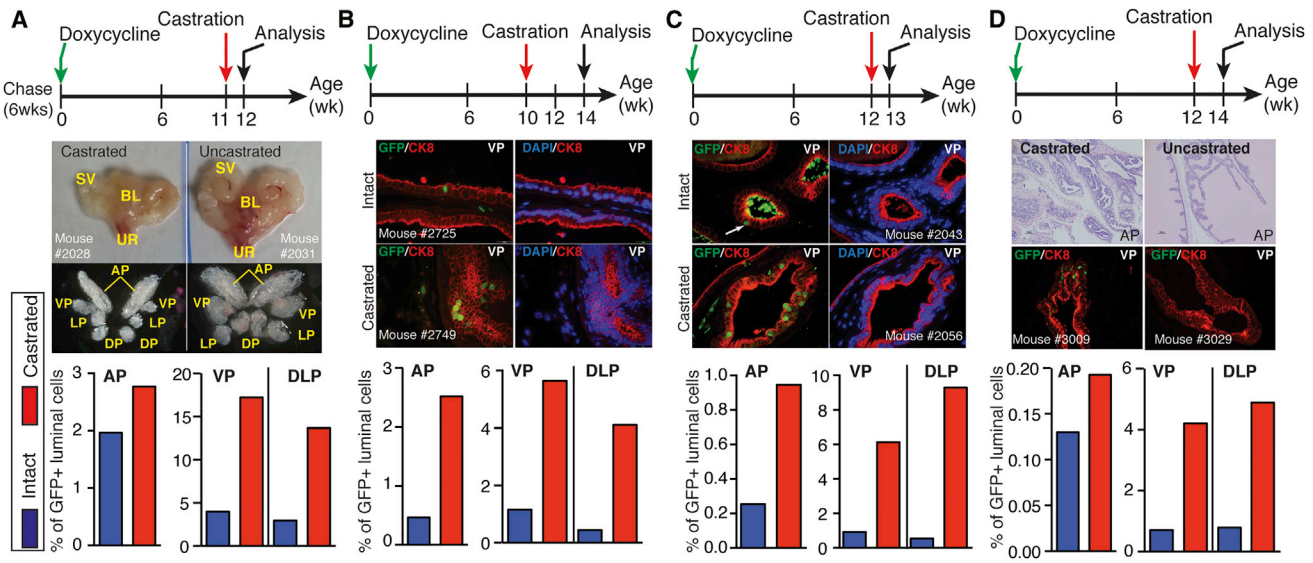

Figure 6. Luminal LRCs Resist Castration *In Vivo*

The Pb-tetVP16-GFP bigenic male mice were castrated at 11, 10, 12, and 12 weeks after chase and analyzed 1 week (A), 4 weeks (B), 1 week (C), and 2 weeks (D) later, respectively. Shown are representative images of urogenital organs and dissected prostate lobes (A), IF of GFP and CK8 in the VP (B–D) and H&E of AP (D) from bigenic mice with or without castration. Quantification of the percentage of GFP^+ cells in $CK8^+$ luminal cell population in different prostate lobes in above experimental castration settings is presented at the bottom. Arrow in (C) indicates a rare GFP^+CK8^+ luminal cell. See also Figure S6.

CK19 was proposed as a prostate luminal progenitor marker in several studies (Hudson et al., 2001; Korsten et al., 2009; Wang et al., 2001) and several SC factors such as BMI1 (Yoo et al., 2016), SOX2 (Kregel et al., 2013), STAT3 (Schroeder et al., 2014), and HOXB9 (de Pinieux et al., 2001) have been associated with stem-like prostate (cancer) cells under castration condition. We performed double IF staining of GFP and about a dozen of reported mouse prostate/mammary luminal progenitor markers on prostate tissues collected from bigenic mice chased for 12 weeks and correlated with the marker mRNA levels in RNA-seq (Figure 7A). Most of these markers were undetectable in normal uncastrated prostates in both formalin-fixed and paraffin-embedded cryosections (Figure 7A). Consistent with the RNA-seq data (Figures 5C and 7A), L-GFP^+ cells expressed relatively abundant CK19 protein compared with L-GFP^- cells, although not all $CK19^{high}$ cells were GFP^+ (Figures 7B and S7A). A subset of L-GFP^+ cells co-expressed SCA-1 at the proximal prostate, and not all $SCA\text{-}1^+$ cells were GFP^+ (Figure 7B), consistent with a recent report that SCA-1 identifies a distinct subset of androgen-independent luminal progenitors in the proximal prostate (Kwon et al., 2016). The 12-week-chased L-GFP^+ cells did not co-localize with BMI1-expressing cells (Figures 7B and S7A), a rare population that mainly resides in the basal cell layer (Lukacs et al., 2010b), although $Bmi1^+$ cells have recently been reported to reside, infrequently, in the luminal layer and mark rare castration-resistant luminal progenitors (Yoo et al., 2016). We detected a relatively low and homogeneous expression of NOTCH1 (Figure 7B), suggesting that, unlike in mammary tissues (Rodilla et al., 2015), NOTCH1 is not a preferential marker for prostate luminal progenitors. The positive staining of BMI1 and SCA-1 in stromal cells, and cleaved caspase-3 in apoptotic cells shed into the lumen after castration, served as positive control for IF analysis (Figure S7B). Together, these data suggest that prostate luminal progenitors are phenotypically, and, likely, functionally (as reflected by heterogeneous AR expression), heterogeneous.

DISCUSSION

Recent studies, employing 2D (Zhang et al., 2017) and 3D organoid (Karthaus et al., 2014) *in vitro* culture systems for human prostate and BrdU pulse-chase (Tsujimura et al., 2002) and lineage-tracing (Choi et al., 2012; Ousset et al., 2012) techniques for murine prostate, have indicated the existence of luminal progenitors within the luminal cell lineage. In this study, we established a bigenic mouse model to specifically label slow-cycling cells in the prostate epithelium, and further defined luminal LRCs as functional progenitors distinct from bulk luminal cells. These luminal LRCs have the following features: (1) they are relatively dormant and, like BrdU-retaining LRCs (Tsujimura et al., 2002), enriched in the proximal prostate; (2) they display

A

	Normalized RC in L-GFP+	FC (L-GFP+/GFP-)	FFPE-IF	OCT-IF	GFP colocalization
Ck19	92518.2768	5.646275064	+	+	+
Notch1	9304.316639	0.488552587	+	+	+
Ly6a/Sca1	424.1028069	0.325800734	+	+	+/-
Bmi1	1511.801771	1.319000165	+	+	-
Cd117/c-Kit	39.9155583	0.105989395	-	-	-
Cd14	922.0493967	0.793129091	-	-	-
Prom1/Cd133	8873.22861	4.055899034	-	-	-
Stat3	11950.71815	0.448870953	-	-	-
Notch3	390.1745824	0.238158347	-	-	-
Cd24	114277.2455	4.360204943	-	-	-
Hoxb9	1540.74055	4.365342588	-	-	-
Sox2	143.6960099	0.136531196	-	-	-

Low mRNA expression RC: readcounts by RNA-seq FC: fold change

B

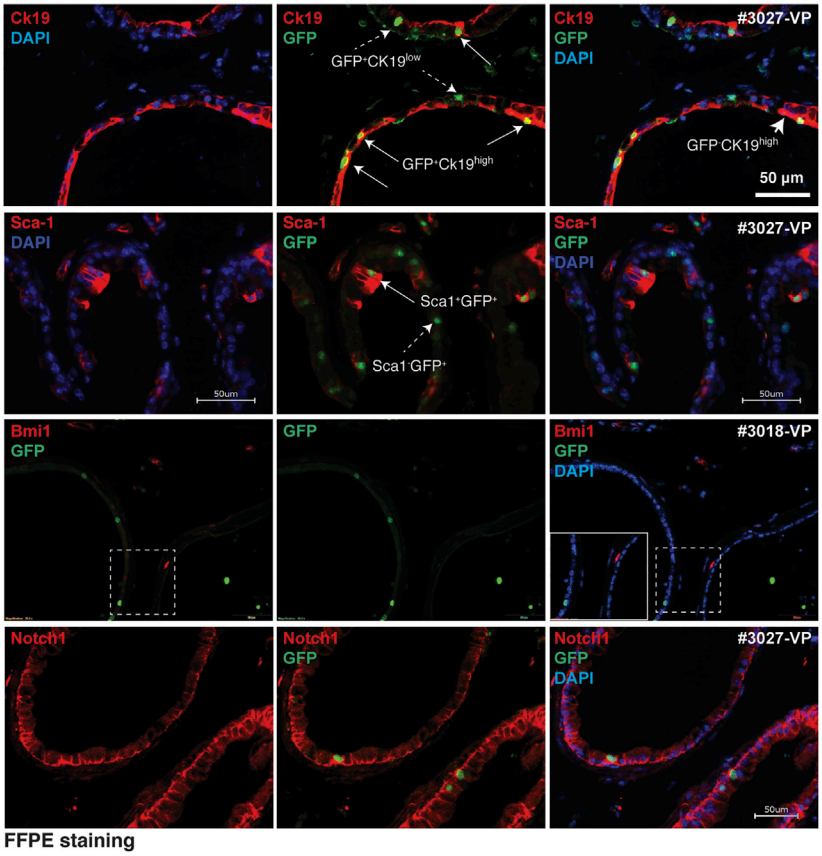

FFPE staining

Figure 7. Phenotypic Heterogeneity of Luminal LRCs

(A) Summary of mRNA (measured in RNA-seq) and protein (measured by IF staining on both frozen and formalin-fixed paraffin-embedded [FFPE] sections) expression of the indicated phenotypic markers of the luminal progenitors.

(B) Double IF staining of GFP and the indicated markers in FFPE sections of prostate glands harvested from bigenic mice chased for 12 weeks. Boxed regions are enlarged. See also Figure S7.

bipotential differentiation ability in both *in vitro* organoid and *in vivo* prostate regeneration assays; (3) they express a progenitor gene signature with preferential expression of neurogenesis- and inflammation-associated genes, and this gene signature is dramatically enriched in treatment-failed PCa; (4) they survive androgen ablation by resisting castration-induced apoptosis and are further enriched in the prostate of castrated mice; and (5) they are phenotypically heterogeneous with only a subset expressing previously reported progenitor markers such as CK19 and SCA-1.

Studying prostatic luminal cells has been challenging due to their low stemness and the current infeasibility of efficient culturing *in vitro*. Prior studies have mainly employed known SC-related surface markers identified in other tissues to dissect the epithelial biology of the prostate. Currently, there is no well-accepted definition for prostate luminal progenitors (Zhang et al., 2017), and only a few studies have reported putative phenotypic markers of stem-like luminal cells in humans (i.e., $CD38^{low}$; Liu et al., 2016) and in regressed mouse prostates (e.g., $NKX3.1^{+}$ [Wang et al., 2009], $SCA\text{-}1^{+}$ [Kwon et al., 2016], and $BMI1^{+}$ [Yoo et al., 2016]). The slow-cycling luminal progenitor (i.e., $L\text{-}GFP^{+}$) cells, identified here in a marker-independent manner, only partially overlap with a few of

previously reported progenitor markers. In fact, most of the markers we analyzed, including CD117, CD14, CD133, STAT3, NOTCH3, CD24, HOXB9, and SOX2, seem to be expressed at too low levels to be reliably detected in the normal mouse prostate. Nevertheless, luminal LRCs appear to generally express low NOTCH1 and high CK19 levels, and a subset of LRCs stains positive for SCA-1. Consistent with a recent report (Yoo et al., 2016) showing that BMI1$^+$ luminal cells are rarely seen in normal prostate, our LRCs do not co-localize with BMI1$^+$ cells. These observations raise a question of whether the mouse prostate, under homeostatic conditions, might have distinct luminal progenitor subsets at varying proliferative states, like the hematopoietic system. For example, our LRCs mainly isolate slow-cycling luminal progenitor cells, while the SCA-1$^+$LRCs$^-$ might represent fast-proliferating luminal progenitors. Regardless, our study, together with studies from others mentioned above, suggests the presence of multiple luminal progenitor cell populations in the unperturbed mouse prostate. Notably, our present study focuses on normal luminal progenitors; whether these LRCs change their phenotypic marker profiles and then overlap with some of the luminal progenitors (e.g., CARNs and CARBs) previously reported in regressed prostate remains to be determined.

Significantly, the slow-cycling LRCs, like NKX3.1-expressing CARNs (Wang et al., 2009), SCA-1$^+$ (Kwon et al., 2016), and BMI1$^+$ (Yoo et al., 2016) luminal progenitors in regressed prostates, are intrinsically resistant to castration, suggesting that the luminal cell layer in normal prostate harbors subsets of naturally androgen-insensitive cells that can survive androgen deprivation. Castration resistance in LRCs could be related to relatively low AR expression, as ~37% LRCs express low levels of AR protein. Simultaneously or alternatively, castration resistance in LRCs may also be associated with their relative quiescence. In this regard, the L-GFP$^+$ cells coordinately underexpress a cohort of positive cell-cycle regulator genes. Detailed dissection of LRCs in castrated prostates is needed to reveal mechanisms of androgen ablation resistance. One potential solution is to perform single-cell RNA-seq analysis to reveal cell-to-cell heterogeneity within the luminal cell compartment under both physiological and castration conditions.

The study of luminal progenitors in the prostate is of great significance to both basic and clinical research. First, luminal cells are the functional units mediating secretory activities and the luminal cell layer is self-sustaining (Choi et al., 2012), indicating the importance of progenitors in maintaining prostate homeostasis and glandular functions (Xie et al., 2017; Zhang et al., 2016a). Second, the luminal layer *in situ* seems to be overall more proliferative (Wang et al., 2013; Zhang et al., 2016b) and murine luminal cells are more susceptible to tumorigenic transformation to generate aggressive tumors (Wang et al., 2014b). This raises the possibility of luminal progenitors functioning as preferred cells-of-origin for CRPC. Our current findings that luminal LRCs preferentially survive androgen ablation provide support to this possibility. Third, stem-like luminal cells may function as tumor-propagating cells (Stoyanova et al., 2013), in line with mouse genetic studies (Abou-Kheir et al., 2010; Korsten et al., 2009) and with previous report showing that aggressive breast basal-like cancers actually originate from luminal progenitors rather than from basal SCs (Molyneux et al., 2010). Fourth, while this manuscript was under revision, a study identified a rare castration-resistant luminal progenitor cell population with a Lin$^-$/SCA-1$^+$/CD49f^{med} phenotype highly enriched in *Pten*-null prostate tumors (Sackmann Sala et al., 2017). Finally, the luminal progenitor gene expression profile can be linked to advanced and aggressive PCa subtypes (Liu et al., 2016; Sackmann Sala et al., 2017; Zhang et al., 2017; this study). This notion is further strengthened by the molecular resemblance of our luminal LRCs to recently reported human CD38^{low} prostatic luminal progenitors (Liu et al., 2016), which has been shown to be associated with inflammation and PCa progression with poor outcome. In aggregate, our study presents a comprehensive biological and molecular characterization of slow-cycling prostate luminal progenitors. Further studies on the functional roles of luminal LRCs in tumorigenesis, and the molecular mechanisms that regulate their homeostasis and dormancy, may yield new predictive markers and therapeutic targets for aggressive CRPC.

EXPERIMENTAL PROCEDURES

General procedures in producing and propagating transgenic animals have been described previously (Suraneni et al., 2010). All animal work was performed under the University of Texas MD Anderson Cancer Center and Roswell Park Cancer Institute IACUC approved protocols. Immunostaining was performed on either paraffin-embedded or OCT frozen sections. The mouse prostate tissues were enzymatically digested with collagenase IA and Dispase, followed by FACS analysis using the BD Aria (BD Biosciences).

Additional experimental procedures are detailed in the Supplemental Experimental Procedures.

ACCESSION NUMBERS

The accession number for the RNA-seq data reported in this paper is GEO: GSE98760.

SUPPLEMENTAL INFORMATION

Supplemental Information includes Supplemental Experimental Procedures, seven figures, and three tables and can be found with this article online at https://doi.org/10.1016/j.stemcr.2017.11.016.

AUTHOR CONTRIBUTIONS

D.Z., C.J., and D.G.T. conceived and designed the study. D.Z., S.G., C.J., and A.T. performed the experiments; D.Z., Y.L., and J.S. performed RNA-seq and bioinformatics analysis. D.Z. and D.G.T. analyzed and interpreted the data. D.Z. and D.G.T. wrote the paper. All authors read and approved the final manuscript.

ACKNOWLEDGMENTS

For the work conducted at the University of Texas MD Anderson Cancer Center (MDACC), we thank the Science Park Animal Core for animal maintenance and care, the Histology Core for IHC studies, P. Whitney for assistance in FACS, Y. Takata for technical help in RNA-seq, and the MDACC Department of Epigenetics and Molecular Carcinogenesis Flow Cytometry and Cell Imaging Core (FCCIC) headed by C.J. For work performed at Roswell Park Cancer Institute (RPCI), we acknowledge the support of several shared resources including flow and image cytometry (K. de Jong) and genomics resources. We thank Dr. J. Kirk for critically reading the manuscript and other Tang lab members for helpful discussions and suggestions. This project was supported by grants from the US NIH (R01-CA155693), Department of Defense (W81XWH-13-1-0352, W81XWH-14-1-0575, and W81XWH-16-1-0575), CPRIT (RP120380), and the Chinese Ministry of Science and Technology (MOST) grant 2016YFA0101203 (all to D.G.T.), and by RPCI and NCI center grant P30CA016056. This study also made use of the Science Park NGS Core, supported by CRPIT Core Facility Support Award RP120348 (to J.S.). We apologize to the colleagues whose work was not cited due to space constraint.

Received: June 23, 2017
Revised: November 22, 2017
Accepted: November 23, 2017
Published: December 21, 2017

REFERENCES

Abou-Kheir, W.G., Hynes, P.G., Martin, P.L., Pierce, R., and Kelly, K. (2010). Characterizing the contribution of stem/progenitor cells to tumorigenesis in the Pten–/–TP53–/– prostate cancer model. Stem Cells *28*, 2129–2140.

Agarwal, S., Hynes, P.G., Tillman, H.S., Lake, R., Abou-Kheir, W.G., Fang, L., Casey, O.M., Ameri, A.H., Martin, P.L., Yin, J.J., et al. (2015). Identification of different classes of luminal progenitor cells within prostate tumors. Cell Rep. *13*, 2147–2158.

Burger, P.E., Xiong, X., Coetzee, S., Salm, S.N., Moscatelli, D., Goto, K., and Wilson, E.L. (2005). Sca-1 expression identifies stem cells in the proximal region of prostatic ducts with high capacity to reconstitute prostatic tissue. Proc. Natl. Acad. Sci. USA *102*, 7180–7185.

Choi, N., Zhang, B., Zhang, L., Ittmann, M., and Xin, L. (2012). Adult murine prostate basal and luminal cells are self-sustained lineages that can both serve as targets for prostate cancer initiation. Cancer Cell *21*, 253–265.

de Pinieux, G., Legrier, M.E., Poirson-Bichat, F., Courty, Y., Bras-Goncalves, R., Dutrillaux, A.M., Némati, F., Oudard, S., Lidereau, R., Broqua, P., et al. (2001). Clinical and experimental progression of a new model of human prostate cancer and therapeutic approach. Am. J. Pathol. *159*, 753–764.

dos Santos, C.O., Rebbeck, C., Rozhkova, E., Valentine, A., Samuels, A., Kadiri, L.R., Osten, P., Harris, E.Y., Uren, P.J., Smith, A.D., and Hannon, G.J. (2013). Molecular hierarchy of mammary differentiation yields refined markers of mammary stem cells. Proc. Natl. Acad. Sci. USA *110*, 7123–7130.

Foudi, A., Hochedlinger, K., Van Buren, D., Schindler, J.W., Jaenisch, R., Carey, V., and Hock, H. (2009). Analysis of histone 2B-GFP retention reveals slowly cycling hematopoietic stem cells. Nat. Biotechnol. *27*, 84–90.

Hudson, D.L., Guy, A.T., Fry, P., O'Hare, M.J., Watt, F.M., and Masters, J.R. (2001). Epithelial cell differentiation pathways in the human prostate: identification of intermediate phenotypes by keratin expression. J. Histochem. Cytochem. *49*, 271–278.

Karthaus, W.R., Iaquinta, P.J., Drost, J., Gracanin, A., van Boxtel, R., Wongvipat, J., Dowling, C.M., Gao, D., Begthel, H., Sachs, N., et al. (2014). Identification of multipotent luminal progenitor cells in human prostate organoid cultures. Cell *159*, 163–175.

Kato, M., Ishii, K., Iwamoto, Y., Sasaki, T., Kanda, H., Yamada, Y., Arima, K., Shiraishi, T., and Sugimura, Y. (2013). Activation of FGF2-FGFR signaling in the castrated mouse prostate stimulates the proliferation of basal epithelial cells. Biol. Reprod. *89*, 81.

Korsten, H., Ziel-van der Made, A., Ma, X., van der Kwast, T., and Trapman, J. (2009). Accumulating progenitor cells in the luminal epithelial cell layer are candidate tumor initiating cells in a Pten knockout mouse prostate cancer model. PLoS One *4*, e5662.

Kregel, S., Kiriluk, K.J., Rosen, A.M., Cai, Y., Reyes, E.E., Otto, K.B., Tom, W., Paner, G.P., Szmulewitz, R.Z., and Vander Griend, D.J. (2013). Sox2 is an androgen receptor-repressed gene that promotes castration-resistant prostate cancer. PLoS One *8*, e53701.

Kwon, O.J., and Xin, L. (2014). Prostate epithelial stem and progenitor cells. Am. J. Clin. Exp. Urol. *2*, 209–218.

Kwon, O.J., Valdez, J.M., Zhang, L., Zhang, B., Wei, X., Su, Q., Ittmann, M.M., Creighton, C.J., and Xin, L. (2014). Increased Notch signalling inhibits anoikis and stimulates proliferation of prostate luminal epithelial cells. Nat. Commun. *5*, 4416.

Kwon, O.J., Zhang, L., and Xin, L. (2016). Stem cell antigen-1 identifies a distinct androgen-independent murine prostatic luminal cell lineage with bipotent potential. Stem Cells *34*, 191–202.

Lafkas, D., Rodilla, V., Huyghe, M., Mourao, L., Kiaris, H., and Fre, S. (2013). Notch3 marks clonogenic mammary luminal progenitor cells in vivo. J. Cell Biol. *203*, 47–56.

Lawson, D.A., Xin, L., Lukacs, R.U., Cheng, D., and Witte, O.N. (2007). Isolation and functional characterization of murine prostate stem cells. Proc. Natl. Acad. Sci. USA *104*, 181–186.

Liu, X., Grogan, T.R., Hieronymus, H., Hashimoto, T., Mottahedeh, J., Cheng, D., Zhang, L., Huang, K., Stoyanova, T., Park, J.W., et al. (2016). Low CD38 identifies progenitor-like inflammation-associated luminal cells that can initiate human prostate cancer and predict poor outcome. Cell Rep. *17*, 2596–2606.

Lukacs, R.U., Goldstein, A.S., Lawson, D.A., Cheng, D., and Witte, O.N. (2010a). Isolation, cultivation and characterization of adult murine prostate stem cells. Nat. Protoc. *5*, 702–713.

Lukacs, R.U., Memarzadeh, S., Wu, H., and Witte, O.N. (2010b). Bmi-1 is a crucial regulator of prostate stem cell self-renewal and malignant transformation. Cell Stem Cell *7*, 682–693.

Molyneux, G., Geyer, F.C., Magnay, F.A., McCarthy, A., Kendrick, H., Natrajan, R., Mackay, A., Grigoriadis, A., Tutt, A., Ashworth, A., et al. (2010). BRCA1 basal-like breast cancers originate from luminal epithelial progenitors and not from basal stem cells. Cell Stem Cell *7*, 403–417.

Ousset, M., Van Keymeulen, A., Bouvencourt, G., Sharma, N., Achouri, Y., Simons, B.D., and Blanpain, C. (2012). Multipotent and unipotent progenitors contribute to prostate postnatal development. Nat. Cell Biol. *14*, 1131–1138.

Pignon, J.C., Grisanzio, C., Geng, Y., Song, J., Shivdasani, R.A., and Signoretti, S. (2013). p63-expressing cells are the stem cells of developing prostate, bladder, and colorectal epithelia. Proc. Natl. Acad. Sci. USA *110*, 8105–8110.

Qin, J., Liu, X., Laffin, B., Chen, X., Choy, G., Jeter, C.R., Calhoun-Davis, T., Li, H., Palapattu, G.S., Pang, S., et al. (2012). The PSA(-/lo) prostate cancer cell population harbors self-renewing long-term tumor-propagating cells that resist castration. Cell Stem Cell *10*, 556–569.

Rodilla, V., Dasti, A., Huyghe, M., Lafkas, D., Laurent, C., Reyal, F., and Fre, S. (2015). Luminal progenitors restrict their lineage potential during mammary gland development. PLoS Biol. *13*, e1002069.

Rycaj, K., and Tang, D.G. (2015). Cell-of-origin of cancer versus cancer stem cells: assays and interpretations. Cancer Res. *75*, 4003–4011.

Sackmann Sala, L., Boutillon, F., Menara, G., De Goyon-Pelard, A., Leprevost, M., Codzamanian, J., Lister, N., Pencik, J., Clark, A., Cagnard, N., et al. (2017). A rare castration-resistant progenitor cell population is highly enriched in Pten-null prostate tumours. J. Pathol. *243*, 51–64.

Salm, S.N., Burger, P.E., Coetzee, S., Goto, K., Moscatelli, D., and Wilson, E.L. (2005). TGF-{beta} maintains dormancy of prostatic stem cells in the proximal region of ducts. J. Cell Biol. *170*, 81–90.

Schroeder, A., Herrmann, A., Cherryholmes, G., Kowolik, C., Buettner, R., Pal, S., Yu, H., Muller-Newen, G., and Jove, R. (2014). Loss of androgen receptor expression promotes a stem-like cell phenotype in prostate cancer through STAT3 signaling. Cancer Res. *74*, 1227–1237.

Shehata, M., Teschendorff, A., Sharp, G., Novcic, N., Russell, I.A., Avril, S., Prater, M., Eirew, P., Caldas, C., Watson, C.J., and Stingl, J. (2012). Phenotypic and functional characterisation of the luminal cell hierarchy of the mammary gland. Breast Cancer Res. *14*, R134.

Shen, M.M., and Abate-Shen, C. (2010). Molecular genetics of prostate cancer: new prospects for old challenges. Genes Dev. *24*, 1967–2000.

Stoyanova, T., Goldstein, A.S., Cai, H., Drake, J.M., Huang, J., and Witte, O.N. (2012). Regulated proteolysis of Trop2 drives epithelial hyperplasia and stem cell self-renewal via beta-catenin signaling. Genes Dev. *26*, 2271–2285.

Stoyanova, T., Cooper, A.R., Drake, J.M., Liu, X., Armstrong, A.J., Pienta, K.J., Zhang, H., Kohn, D.B., Huang, J., Witte, O.N., and Goldstein, A.S. (2013). Prostate cancer originating in basal cells progresses to adenocarcinoma propagated by luminal-like cells. Proc. Natl. Acad. Sci. USA *110*, 20111–20116.

Suraneni, M.V., Schneider-Broussard, R., Moore, J.R., Davis, T.C., Maldonado, C.J., Li, H., Newman, R.A., Kusewitt, D., Hu, J., Yang, P., and Tang, D.G. (2010). Transgenic expression of 15-lipoxygenase 2 (15-LOX2) in mouse prostate leads to hyperplasia and cell senescence. Oncogene *29*, 4261–4275.

Szotek, P.P., Chang, H.L., Brennand, K., Fujino, A., Pieretti-Vanmarcke, R., Lo Celso, C., Dombkowski, D., Preffer, F., Cohen, K.S., Teixeira, J., and Donahoe, P.K. (2008). Normal ovarian surface epithelial label-retaining cells exhibit stem/progenitor cell characteristics. Proc. Natl. Acad. Sci. USA *105*, 12469–12473.

Tang, D.G. (2012). Understanding cancer stem cell heterogeneity and plasticity. Cell Res. *22*, 457–472.

Tsujimura, A., Koikawa, Y., Salm, S., Takao, T., Coetzee, S., Moscatelli, D., Shapiro, E., Lepor, H., Sun, T.T., and Wilson, E.L. (2002). Proximal location of mouse prostate epithelial stem cells: a model of prostatic homeostasis. J. Cell Biol. *157*, 1257–1265.

Tumbar, T., Guasch, G., Greco, V., Blanpain, C., Lowry, W.E., Rendl, M., and Fuchs, E. (2004). Defining the epithelial stem cell niche in skin. Science *303*, 359–363.

Valdez, J.M., Zhang, L., Su, Q., Dakhova, O., Zhang, Y., Shahi, P., Spencer, D.M., Creighton, C.J., Ittmann, M.M., and Xin, L. (2012). Notch and TGFbeta form a reciprocal positive regulatory loop that suppresses murine prostate basal stem/progenitor cell activity. Cell Stem Cell *11*, 676–688.

Wang, Y., Hayward, S., Cao, M., Thayer, K., and Cunha, G. (2001). Cell differentiation lineage in the prostate. Differentiation *68*, 270–279.

Wang, S., Garcia, A.J., Wu, M., Lawson, D.A., Witte, O.N., and Wu, H. (2006). Pten deletion leads to the expansion of a prostatic stem/progenitor cell subpopulation and tumor initiation. Proc. Natl. Acad. Sci. USA *103*, 1480–1485.

Wang, X., Kruithof-de Julio, M., Economides, K.D., Walker, D., Yu, H., Halili, M.V., Hu, Y.P., Price, S.M., Abate-Shen, C., and Shen, M.M. (2009). A luminal epithelial stem cell that is a cell of origin for prostate cancer. Nature *461*, 495–500.

Wang, Y., Sacchetti, A., van Dijk, M.R., van der Zee, M., van der Horst, P.H., Joosten, R., Burger, C.W., Grootegoed, J.A., Blok, L.J., and Fodde, R. (2012). Identification of quiescent, stem-like cells in the distal female reproductive tract. PLoS One *7*, e40691.

Wang, Z.A., Mitrofanova, A., Bergren, S.K., Abate-Shen, C., Cardiff, R.D., Califano, A., and Shen, M.M. (2013). Lineage analysis of basal epithelial cells reveals their unexpected plasticity and supports a cell-of-origin model for prostate cancer heterogeneity. Nat. Cell Biol. *15*, 274–283.

Wang, J., Zhu, H.H., Chu, M., Liu, Y., Zhang, C., Liu, G., Yang, X., Yang, R., and Gao, W.Q. (2014a). Symmetrical and asymmetrical division analysis provides evidence for a hierarchy of prostate epithelial cell lineages. Nat. Commun. *5*, 4758.

Wang, Z.A., Toivanen, R., Bergren, S.K., Chambon, P., and Shen, M.M. (2014b). Luminal cells are favored as the cell of origin for prostate cancer. Cell Rep. *8*, 1339–1346.

Xie, Q., Liu, Y., Cai, T., Horton, C., Stefanson, J., and Wang, Z.A. (2017). Dissecting cell-type-specific roles of androgen receptor in prostate homeostasis and regeneration through lineage tracing. Nat. Commun. *8*, 14284.

Xin, L., Lawson, D.A., and Witte, O.N. (2005). The Sca-1 cell surface marker enriches for a prostate-regenerating cell subpopulation that can initiate prostate tumorigenesis. Proc. Natl. Acad. Sci. USA *102*, 6942–6947.

Yoo, Y.A., Roh, M., Naseem, A.F., Lysy, B., Desouki, M.M., Unno, K., and Abdulkadir, S.A. (2016). Bmi1 marks distinct castration-resistant luminal progenitor cells competent for prostate regeneration and tumour initiation. Nat. Commun. *7*, 12943.

Zhang, J., Thomas, T.Z., Kasper, S., and Matusik, R.J. (2000). A small composite probasin promoter confers high levels of prostate-specific gene expression through regulation by androgens and glucocorticoids in vitro and in vivo. Endocrinology *141*, 4698–4710.

Zhang, B., Kwon, O.J., Henry, G., Malewska, A., Wei, X., Zhang, L., Brinkley, W., Zhang, Y., Castro, P.D., Titus, M., et al. (2016a). Non-cell-autonomous regulation of prostate epithelial homeostasis by androgen receptor. Mol. Cell *63*, 976–989.

Zhang, D., Park, D., Zhong, Y., Lu, Y., Rycaj, K., Gong, S., Chen, X., Liu, X., Chao, H.P., Whitney, P., et al. (2016b). Stem cell and neurogenic gene-expression profiles link prostate basal cells to aggressive prostate cancer. Nat. Commun. *7*, 10798.

Zhang, D., Lin, K., Lu, Y., Rycaj, K., Zhong, Y., Chao, H.P., Calhoun-Davis, T., Shen, J., and Tang, D.G. (2017). Developing a novel two-dimensional culture system to enrich human prostate luminal progenitors that can function as a cell of origin for prostate cancer. Stem Cells Transl. Med. *6*, 748–760.

Stem Cell Reports, Volume *10*

Supplemental Information

Histone 2B-GFP Label-Retaining Prostate Luminal Cells Possess Progenitor Cell Properties and Are Intrinsically Resistant to Castration

Dingxiao Zhang, Collene Jeter, Shuai Gong, Amanda Tracz, Yue Lu, Jianjun Shen, and Dean G. Tang

Supplementary Data

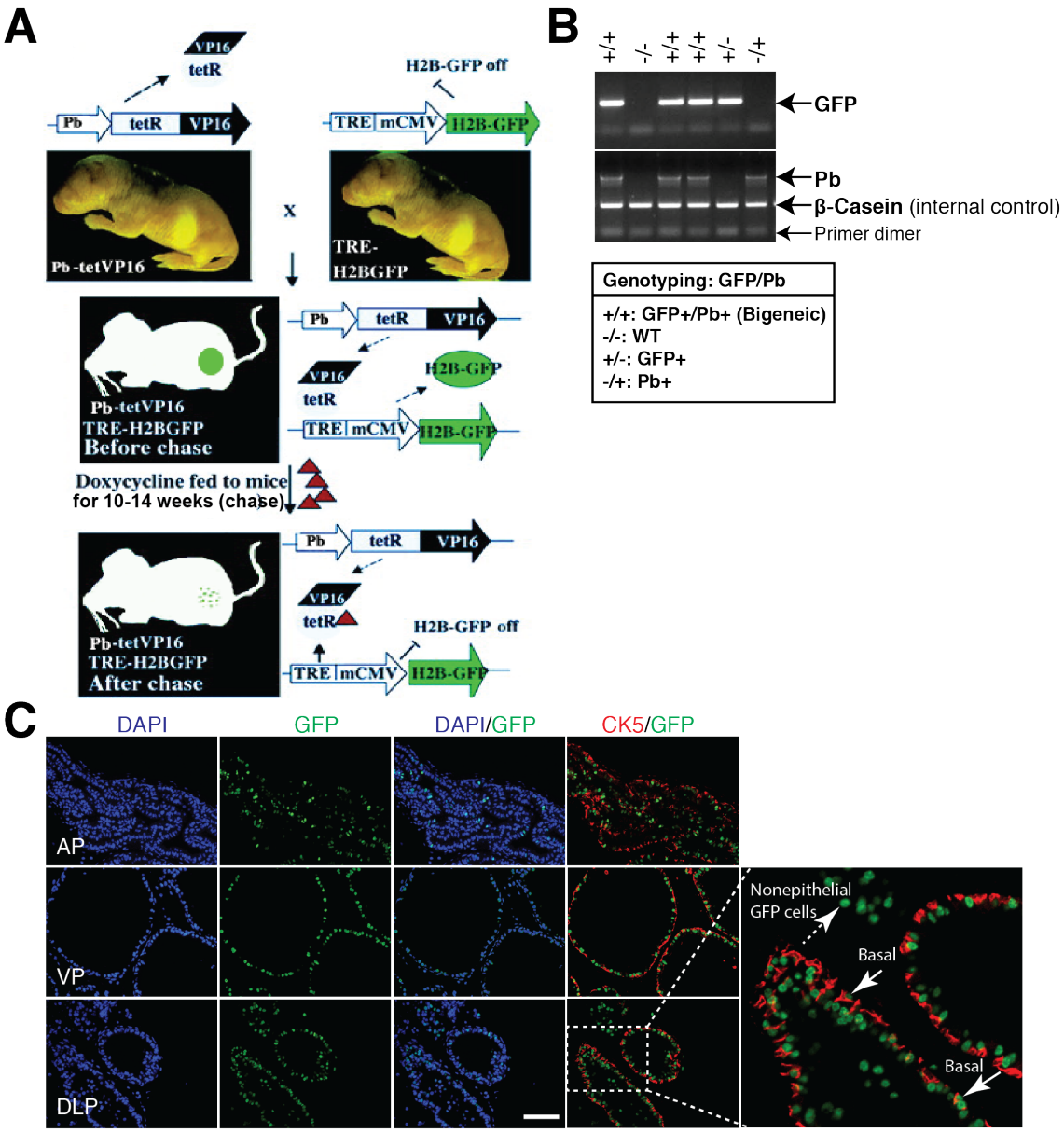

Figure S1. Establishment of a bigenic mouse model to label slow-cycling cells (LRCs) in the prostatic epithelium, Related to Figure 1

(A) Strategy to generate Pb-tetVP16-GFP bigenic mouse model (see Supplemental Experimental Procedures for detail).

(B) PCR genotyping of single and bigenic Pb-tetVP16-GFP mice.

(C) IF staining of CK5 and GFP in different prostate lobes dissected from unchased adult bigenic mouse identifying GFP^{+} basal cells and nonepithelial stromal cells. Boxed regions are enlarged. Scale bar, 100 μm.

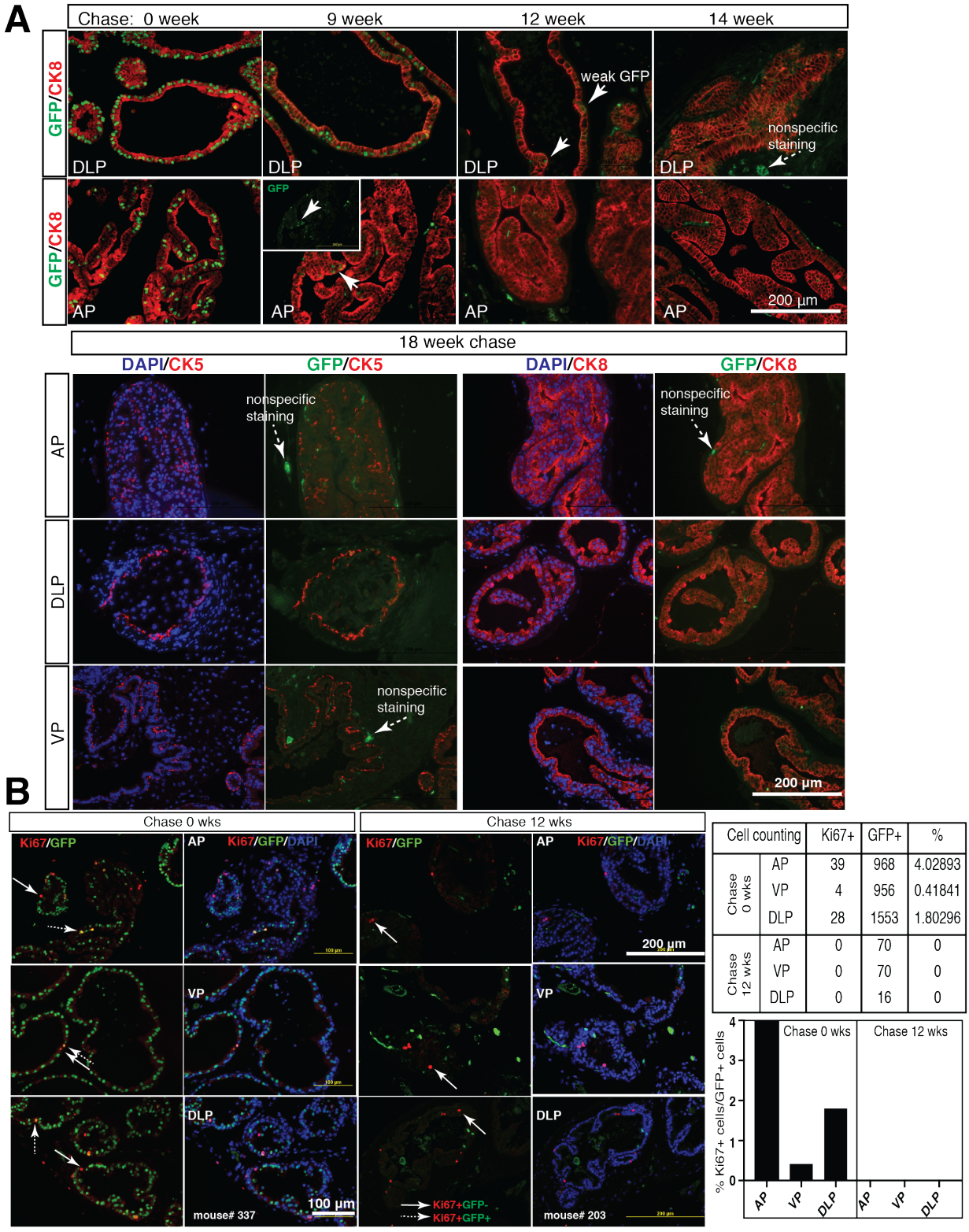

Cell counting		Ki67+	GFP+	%
Chase 0 wks	AP	39	968	4.02893
	VP	4	956	0.41841
	DLP	28	1553	1.80296
Chase 12 wks	AP	0	70	0
	VP	0	70	0
	DLP	0	16	0

Figure S2. Phenotypic characterization and quiescence of prostate LRCs, Related to Figure 2

(A) Double IF staining of CK5 or CK8 and GFP in different prostate lobes harvested from bigenic mice chased for 0 - 18 weeks. Arrows and dashed arrows indicate positive and non-specific GFP staining, respectively.

(B) Double IF of Ki67 and GFP in different prostate lobes of bigenic mice chased for 0 week and 12 weeks. Representative low-magnification images (left) and quantification data (right) are shown. Arrows and dashed arrows indicate $Ki67^{+}GFP^{-}$ single positive and $Ki67^{+}GFP^{+}$ double positive cells, respectively.

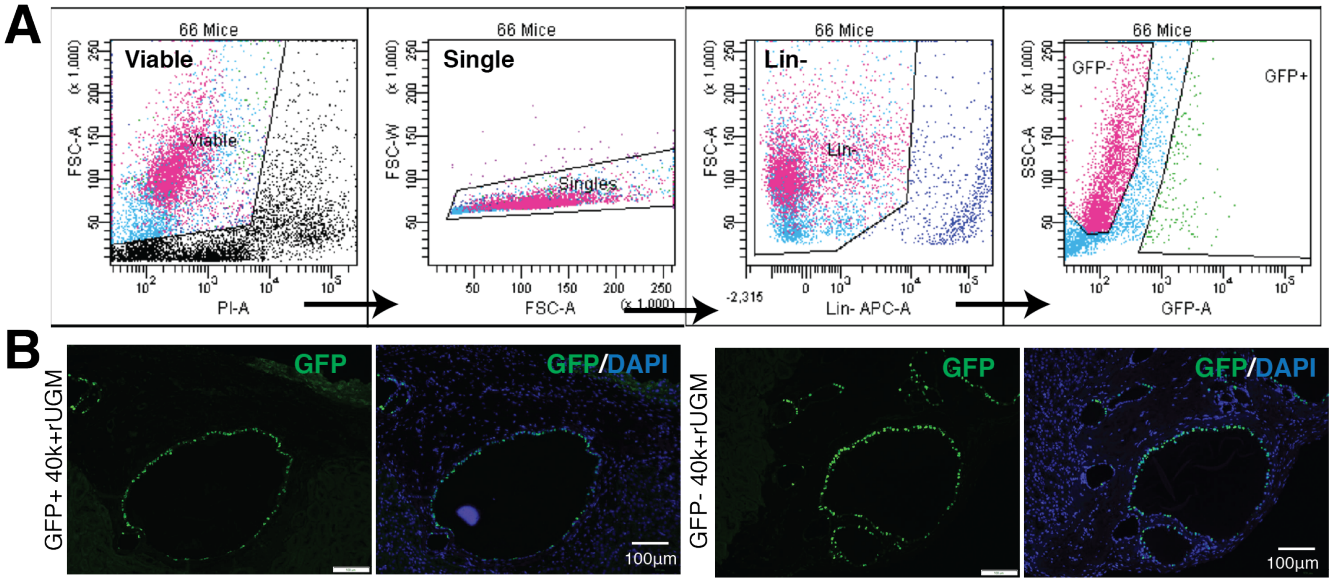

Figure S3. LRCs can regenerate prostate glands *in vivo*, Related to Figure 3

(A) Sorting strategy to isolate lineage-negative GFP^+ and GFP^- cells from disassociated bulk prostatic cells.

(B) IF of GFP in recombinants showing that both LRCs and non-LRCs can regenerate prostate tissues *in vivo*. Note that as we used a Tet-off system, the GFP^- cells isolated from 12-week chased animals (non-LRCs) would regain the GFP expression during the tissue regeneration assays.

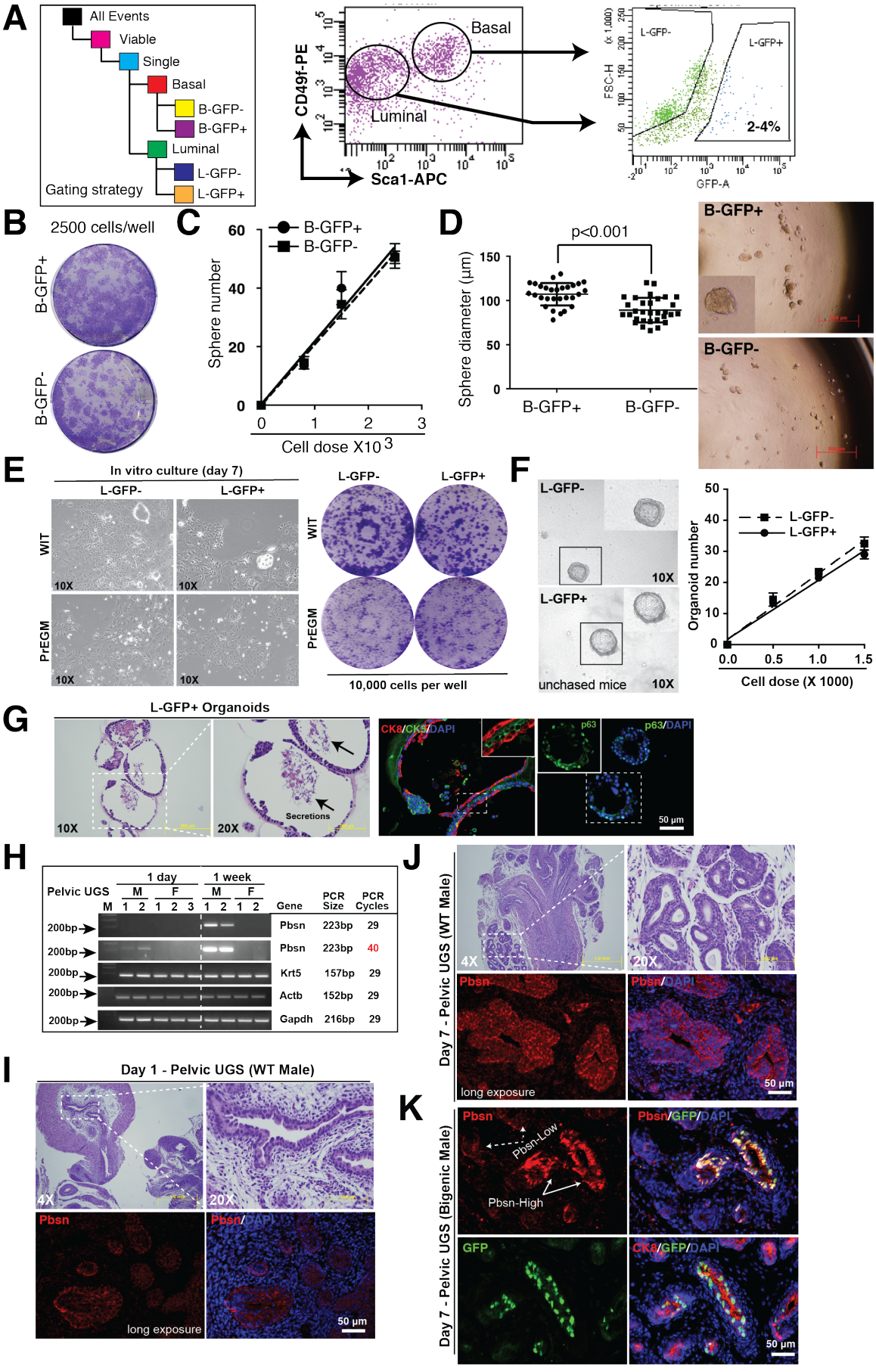
A
All Events
Viable
Single
Basal
B-GFP-
B-GFP+
Luminal
L-GFP-
L-GFP+
Gating strategy
CD49f-PE
Sca1-APC
Basal
Luminal
FSC-H
GFP-A
L-GFP-
L-GFP+
2-4%
B
2500 cells/well
B-GFP+
B-GFP-
C
B-GFP+
B-GFP-
Sphere number
Cell dose X10 3
D
p<0.001
Sphere diameter (µm)
B-GFP+
B-GFP-
B-GFP+
B-GFP-
E
In vitro culture (day 7)
L-GFP-
L-GFP+
WIT
PrEGM
10X
L-GFP-
L-GFP+
WIT
PrEGM
10,000 cells per well
F
L-GFP-
L-GFP+
10X
unchased mice
Organoid number
Cell dose (X 1000)
G
L-GFP+ Organoids
10X
20X
Secretions
CK8/CK5/DAPI
p63
p63/DAPI
50 µm
H
Pelvic UGS
1 day
1 week
M
F
Gene
PCR Size
PCR Cycles
200bp
Pbsn 223bp 29
Pbsn 223bp 40
Krt5 157bp 29
Actb 152bp 29
Gapdh 216bp 29
I
Day 1 - Pelvic UGS (WT Male)
4X
20X
Pbsn
Pbsn/DAPI
long exposure
50 µm
J
Day 7 - Pelvic UGS (WT Male)
4X
20X
Pbsn
Pbsn/DAPI
long exposure
50 µm
K
Day 7 - Pelvic UGS (Bigenic Male)
Pbsn
Pbsn-Low
Pbsn-High
Pbsn/GFP/DAPI
GFP
CK8/GFP/DAPI
50 µm

Figure S4. Luminal LRCs, but not basal LRCs, exhibit preferential stem/progenitor activities compared to non-LRCs, Related to Figure 4

(A) FACS strategy to isolate GFP^+ and GFP^- epithelial cells form both basal and luminal cell populations.

(B-D) Basal GFP^+ LRCs demonstrate similar sphere-forming efficiency to basal GFP^- non-LRCs. Freshly purified Lin^- prostate basal GFP^+/GFP^- cells ($B\text{-}GFP^+/B\text{-}GFP^-$) from 12 week-chased animals were used in colony formation (B) and limiting dilution sphere (C) assays. Note that $B\text{-}GFP^+$ cells did generate larger spheres than $B\text{-}GFP^-$ cells (D). Results shown were representative data of at least 2 independent experiments. The P value was calculated using Student's t-test. For (C) and (D), data represent mean ± SD of values obtained from one experiment.

(E, F) Freshly purified luminal GFP^+ and GFP^- cells from unchased adult animals exhibit similar stem/progenitor cell activities. Shown are 2D colony formation (E) and 3D organoid (F) assays. Pictures in E (left panel) confirmed the epithelial identify of the cells cultured in the indicated medium. Results shown were representative data of at least 2 independent experiments.

(G) Luminal LRCs isolated from 12 week-chased bigenic mice generated organoids containing both basal and luminal cells. Shown are H&E staining and IF analysis of p63, CK5 and CK8 in organoids.

(H) Semi-quantitative RT-PCR of *Pbsn* mRNA in pelvic urogenital sinus (UGS) isolated from newborn and 1-week old mice.

(I, J) H&E staining and IF analysis of Pbsn in pelvic UGS of newborn (I) and 1-week old WT mice (J) showing the minimal and considerable expression of Pbsn at protein level in newborn and 1-week old mice, respectively.

(K) Double IF analysis of GFP and Pbsn or CK8 in pelvic UGS of 1-week old bigenic mice.

Boxed regions are enlarged.

A

	RNA-seq	
	L_GFP-	L_GFP+
total number of fragments	73665989	80259391
fragments with both ends mapped	64184312	69737172
	87%	87%
fragments with one end mapped	4332527	4982840
	6%	6%
tags that are not mapped	14630827	16061598
total mapped rate	93%	93%

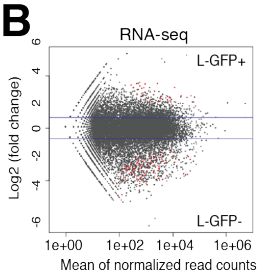

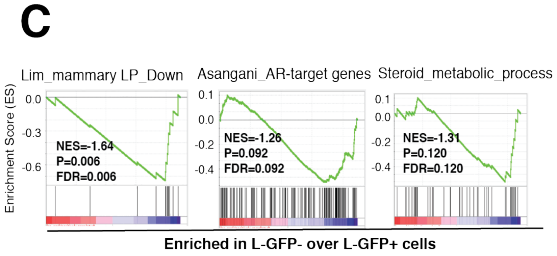

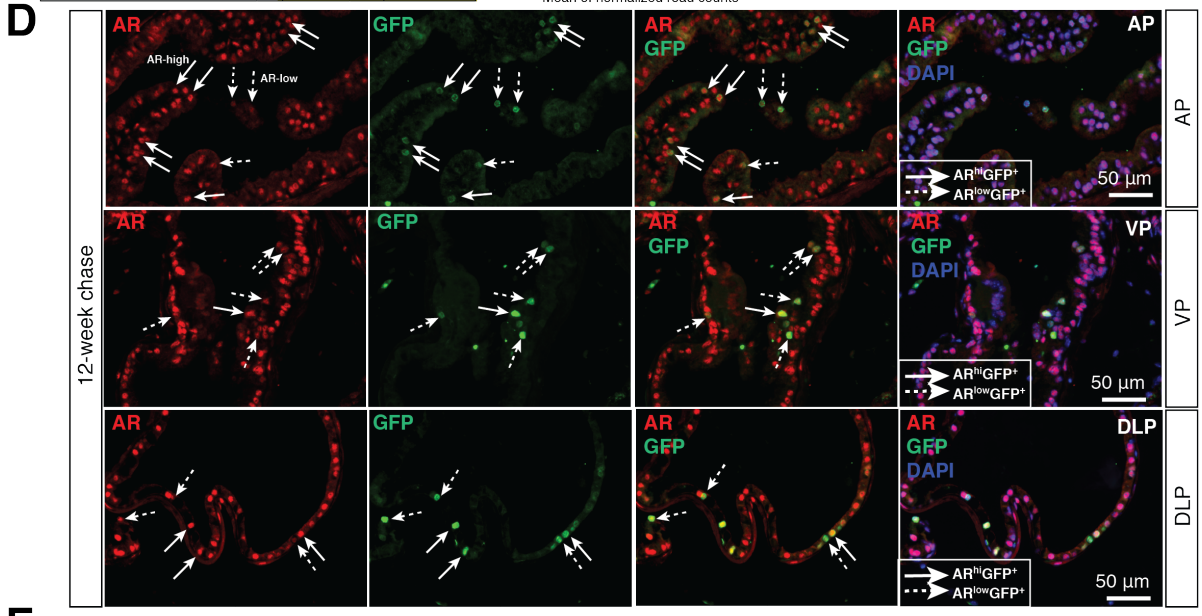

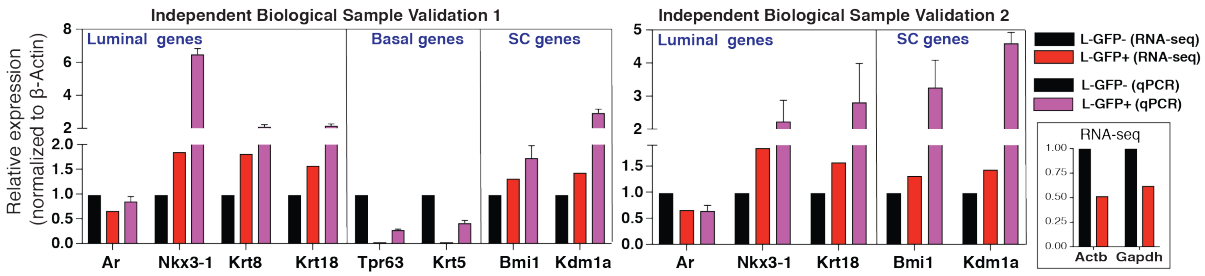

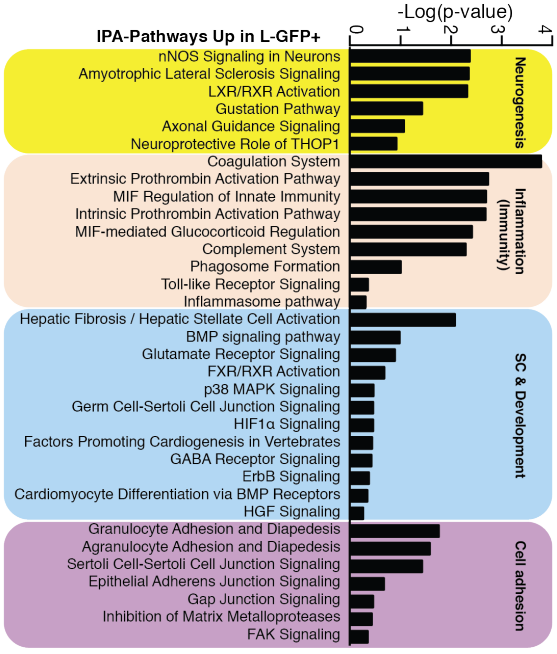

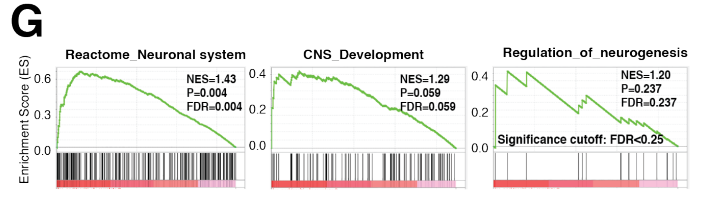

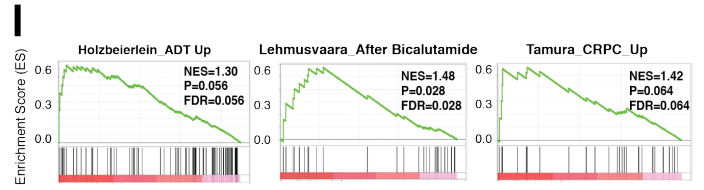

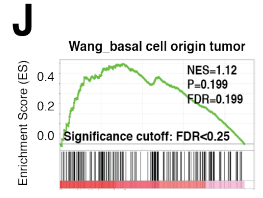

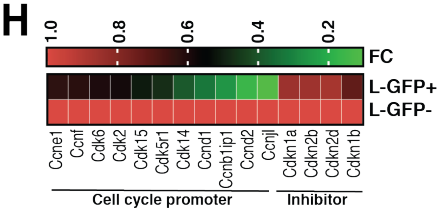

Figure S5. Luminal LRCs express unique progenitor cell gene signatures linked to CRPC, Related to Figure 5

(A) RNA-seq statistics.

(B) The MA plot showing appropriate normalization of our RNA-seq data.

(C) GSEA results showing the enrichment of indicated gene signatures in luminal GFP^- cells.

(D) Double IF staining of GFP and AR in prostates isolated from 12-week chased bigenic animals. Solid arrows point to GFP^+/AR^{hi} cells and dashed arrows to $GFP^{+/}AR^{low}$ cells.

(E) qRT-PCR validation of RNA-seq data. Two independently prepared sample pairs (luminal GFP^+ and GFP^- cells) were used in qRT-PCR analysis of several representative genes in 'luminal', 'basal', and 'SC' categories. Overall, the trend of gene expression was consistent between these two measurements with more dramatic differences detected by qPCR, which is reasonable as qPCR utilized Actb as normalization and tended to be more quantitative while RNA-seq did not use housekeeping gene expression for normalization. Note that both Actb and Gapdh mRNA expression levels were not evenly distributed in the L-GFP^+ and L-GFP^- cell populations in RNA-seq analysis (right boxed). Gene expression values in L-GFP^- cells detected by qPCR or RNA-seq were arbitrarily set as 1 for the purpose of comparison.

(F) Ingenuity pathway analysis (IPA) of genes preferentially upregulated in luminal GFP^+ cells.

(G) GSEA results showing the enrichment of indicated gene signatures in luminal GFP^+ cells.

(H) Heatmap of representative cell-cycle regulators in luminal GFP^+ and GFP^- cells. The relative gene expression values (i.e., fold change, FC) in L-GFP^+ over GFP- (arbitrarily set as 1) were used.

(I, J) GSEA results showing the enrichment of indicated gene signatures in luminal GFP^+ cells. Note that an FDR < 0.25 is statistically significant for GSEA analysis.

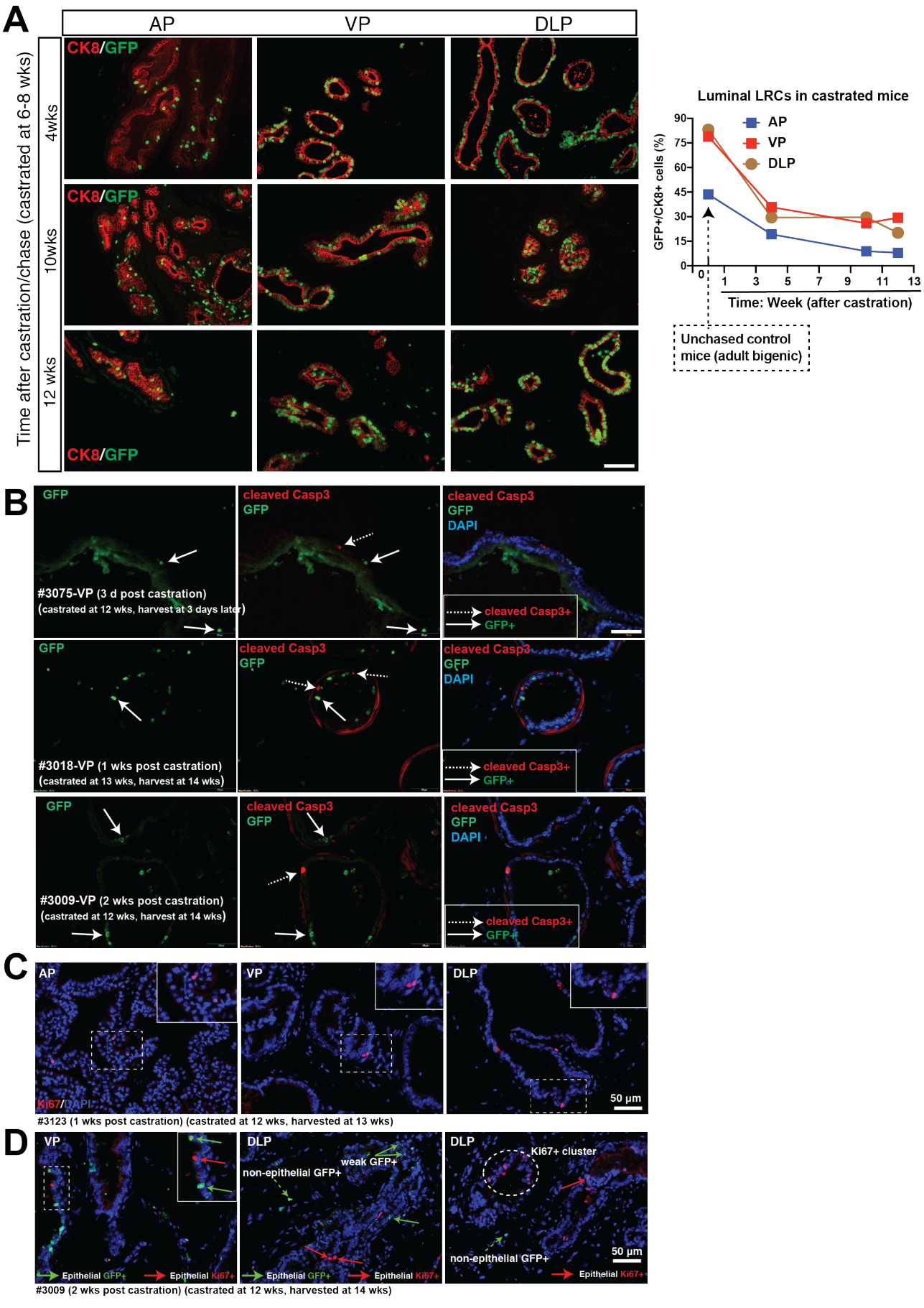
A
AP
VP
DLP
Time after castration/chase (castrated at 6-8 wks)
4wks
10wks
12 wks
CK8/GFP
Luminal LRCs in castrated mice
AP
VP
DLP
GFP+/CK8+ cells (%)
Time: Week (after castration)
Unchased control mice (adult bigenic)
B
GFP
cleaved Casp3
DAPI
#3075-VP (3 d post castration)
(castrated at 12 wks, harvest at 3 days later)
cleaved Casp3+
GFP+
#3018-VP (1 wks post castration)
(castrated at 13 wks, harvest at 14 wks)
#3009-VP (2 wks post castration)
(castrated at 12 wks, harvest at 14 wks)
C
AP
VP
DLP
Ki67/DAPI
50 μm
#3123 (1 wks post castration) (castrated at 12 wks, harvested at 13 wks)
D
non-epithelial GFP+
weak GFP+
Ki67+ cluster
Epithelial GFP+
Epithelial Ki67+
#3009 (2 wks post castration) (castrated at 12 wks, harvested at 14 wks)

Figure S6. Luminal LRCs mark androgen-independent cells and resist castration-induced apoptosis *in vivo*, Related to Figure 6

(A) Representative IF images and quantification of CK8 and GFP in different prostate lobes harvested from bigenic male mice castrated at 6-8 weeks and chased for 4, 10 and 12 weeks.

(B) IF of cleaved Caspase 3 and GFP in prostate tissues harvested from castrated mice. Different experimental settings, i.e., mice chased for 12 weeks were castrated and VP lobes harvested 3 days (top) or 2 weeks (bottom) later, or castrated at 13 weeks of chase and harvested 1 week later (middle panels) were employed to show that GFP^+ luminal LRCs were apoptosis-negative.

(C) IF of Ki67 in prostate tissues harvested from indicated castrated mice.

(D) IF of GFP and Ki67 in prostate tissues harvested from indicated castrated mice.

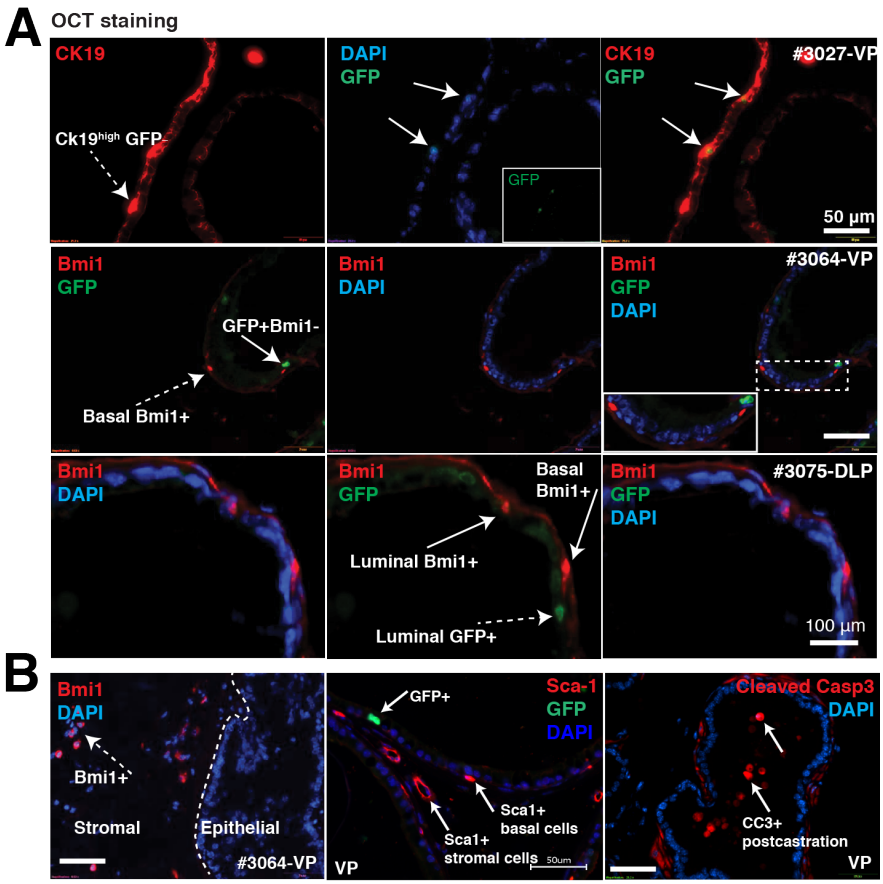

Figure S7. Phenotypic heterogeneity of luminal progenitor cells, Related to Figure 7

(A) Double IF staining of GFP and the indicated markers in frozen sections of prostate glands harvested from bigenic mice chased for 12 weeks. In the middle (right panel), the dashed boxed region is enlarged.

(B) Double IF of GFP and Bmi1 (left panel) or Sca-1 (middle panel) in FFPE sections obtained from bigenic mice chased for 12 weeks, and of GFP and cleaved Caspase 3 (CC3) in frozen tissue sections of prostate isolated from adult bigenic mice castrated for 1 week (right panel).

Table S1. Supporting data for quantitation of GFP^+ cell properties, Related to Figure 2, 4, 5, 6, S2, S6

Table S2. List of the differentially expressed genes (DEGs) in luminal GFP^- and GFP^+ cells (comparative to each other) isolated from 12-week chased bigenic mice in the RNA-Seq analysis, Related to Figure 5 and S5

Table S3. Antibodies and primers used in this study,
Related to Figure 1, 2, 4, 5, 6, 7, S1, S2, S3, S4, S5, S6, S7

Antibody	Supplier	Catalog. No	Species	Dilution
AR	EMD Millipore	06-680	Rabbit	1:750
Ck8	Developmental Studies Hybridoma Bank	TROMA-1	Rat	1:50
Ck5	Covance	PRB-1609	Rabbit	1:500
p63	Cell Signaling	4892S	Rabbit	1:500
Ki67	Leica Biosystems	NCL-Ki67p	Rabbit	1:500
Sox2	Cell Signaling	14962	Rabbit	1:150
GFP	Sigma	G6539	Mouse	1:500
GFP	Life Technologies	A-11122	Rabbit	1:1000
Ck19	Abcam	ab52625	Rabbit	1:200
Notch1	Abcam	ab52627	Rabbit	1:100
Stat3	Abcam	ab76315	Rabbit	1:150
Sca1	Abcam	ab109211	Rabbit	1:100
Cd117/c-Kit	Biolegend	105801	Rat	1:150
Cd14	Biolegend	150101	Rat	1:150
Cd133	Biolegend	141201	Rat	1:100
Notch3	R&D System	AF1308	Goat	1:100
Cd24	Santa cruz	sc-19585	Mouse	1:150
Bmi1	Millipore	05-637	Mouse	1:100
Hoxb9	Assay Biotech	C10404	Rabbit	1:150
Pbsn (M-18)	Santa Cruz	sc-17124	Goat	1:100
Casp3-cleaved	Cell Signaling	9664	Rabbit	1:150

Primer Name	Sequence (Forward 5'-3')	Sequence (Reverse 5'-3')
mGapdh	ATCACTGCCACCCAGAAGAC	AGGTTTCTCCAGGCGGCAC
mActb	AGCAAGCAGGAGTACGATGAG	AAGCCATGCCAATGTTGTC
mPbsn	TGCACAGTATGAAGGGAGCAT	GTCCGTGTCCATGATACGCT
mKrt5	GGGTCTTGGTTTGGGTAGCG	AGGCTCTTCTTAGCTCTTGAAG
mKrt14	GGAGATGATCGGCAGTGTGG	GAAGATGAAAGGTGGGCGT
mTrp63	GCTGCGTCGGAGGAATGAAC	TTGCTGCTTTCTGATGCTGTC
mKrt8	ACACTTTCAGCCGCACCAC	TCTCCCCGTGAGCCCTGA
mKrt18	GAGACGCACCCTCCAGACCT	GCTCCATCTGTGCCTTGTATC
mAr	GACCTGCTAATCAAGTCCCAT	ATTAGGGTTTCCAAATCTTCAC
mBmi1	TTATCAGCCATCAGTTATTTGTG	ACAGCAATGTGTGTAAAAGTAATG
mBcl2	CTACCGTCGTGACTTCGCAG	ACACACATGACCCCACCGA
mAldh1a1	TCAAGACAGTCGCAATGAAGAT	AAAACACGACTATGCTGGTTACTA
mAldh3a1	AGACATCAAGCGGTGGAGTG	AGACCTCACCAGGCAAGAGC
mLy6a	CAGCAGTTATTGTGGATTCTCA	CCTCCATTGGGAACTGCTAC
mNKX3-1	TCCCACCACTCAGTGCTATACAG	AACAAGGGACACGGAACAATAC
mVIM	AGCTGCTAACTACCAGGACACTA	CAGAGGAAGTGACTCCAGGTTAG
mSetdb1	TCAACCAACATGGCTTCCGT	CACCCAAGGGAAGCGAAGA
mKdm1a	GTATCTCGTTGGCGTGCTG	GCCCACTCAACAGAGCACCA
mCtnnb1	CCACCCTGGTGCTGACTATC	ATTTACAGGTCAGTATCAAACCAG

Note: "m" means mouse.

Supplemental Experimental Procedures

Generation of Prostate-Specific Pb-tetVP16-GFP Transgenic Mice

General procedures in producing and propagating transgenic animals have been previously described (Suraneni et al., 2010). Briefly, we adopted a modified tetracycline-repressible histone H2B-GFP (Tet-off) system previously used to assess slow-cycling stem cells in the skin (Tumbar et al., 2004) to monitor GFP dynamics as readout of cell cycle frequency in prostate epithelial cells. Transgene constructs (Figure S1A) were prepared by placing tetR-VP16 (pTET-Off, BD Biosciences Clontech) under the control of prostate specific and androgen responsive composite *probasin* promoter ARR2PB (Zhang et al., 2000) with an intervening rabbit b-globin second intron sequence to augment transgene expression and followed by b-globin–SV40 hybrid polyA sequences for transcript stability (Chen et al., 2009). This ARR2PB-tetR-VP16 line were bred with tetO-HIST1H2BJ/GFP (H2B-GFP) mice (stock # 005104, Jackson Laboratory), in which expression of H2B-GFP is under the control of the TET response element (TRE), to generate Pb-tetVP16-GFP bigenic mice (Figure S1A). To analyze the decay of H2B-GFP signal, young adult bigenic male mice were fed DOX chow (2 g/kg body weight, Teklad) starting at 6 weeks and were kept on DOX food for entire chase period (6-18 weeks).

Colony and Sphere Formation Assays

For colony formation assays (Zhang et al., 2011; Zhang et al., 2016), we plated freshly purified prostate epithelial cells at a low density (i.e., 1,000-10,000 cells/well) in 6-well plate precoated with PureCol (Advanced BioMatrix, San Diego, CA), and let cells grow for 7-10 days before the visualization of the culture by crystal violet staining. For sphere-formation assays (Liu et al., 2011), cells were suspended in 1:1 Matrigel (BD Biosciences, San Jose, CA)/medium in a total volume of 100 µl. The mixtures were then plated around the rims of wells in a 12-well plate and allowed to solidify in 37°C incubator for 25 minutes, followed by addition of 1 ml of warm medium. Usually 7-9 days after plating, spheres with a diameter over 50 µm were counted. PrEGM and modified WIT medium capable of propagating prostatic stem-like cells (inducing luminal progenitors) was used for 2D culture (Zhang et al., 2017) whereas both WIT and recently established prostate organoid medium (Karthaus et al., 2014) were used for 3D sphere/organoid cultures. For all experiments, we ran a minimum of triplicate wells for each condition and repeated experiments 2-4 times.

Histology, Immunofluorescence (IF) Staining, and Microscopy

Hematoxylin and eosin (H&E) and IF staining was performed on either 5-µm paraffin-embedded or OCT frozen sections. Basic IF procedures have been described previously (Jeter et al., 2009). The coverslips or the tissue slides were blocked with Background Sniper (Biocare Medical, Concord, CA) for 30 minutes, followed by primary antibody incubation overnight at 4°C. Primary antibodies and dilutions used are listed in Table S3. Slides were then incubated with secondary antibodies (diluted 1:700 in antibody diluent (Dako, Carpinteria, CA)) labeled with AlexaFluor 488 or 594 (Invitrogen/Molecular Probes, Grand Island, NY). After washing (3X) with PBS, sections were counterstained with 4,6-diamidino-2-phenylindole (DAPI) (Sigma-Aldrich, St. Louis, MO) and mounted with ProLong® Gold Antifade Mountant (Life Technologies, Grand Island, NY). For quantification of AR staining intensity in luminal GFP^+ cells, a serial dilution of AR antibody from 1:100 to 1:750 was tested and 1:750 dilutions was selected. H&E and IF images were captured by Olympus IX71, and Keyence BZ-X700 and Zeiss LSM510 META confocal microscope, respectively.

Mouse Prostate Tissue Disassociation and Flow Cytometry

Prostate tissues were dissected and minced to small clumps, followed by enzymatic dissociation with collagenase IA (200 U/ml) and Dispase (1 U/ml) in DMEM media with 10% FBS and 10 µM of p160ROCK inhibitor Y-27632 dihydrochloride (Selleckchem, Houston, TX) for 90 min. Dissociated tissue was then treated with 0.2% Trypsin for 10 min followed by 35 min DNase I (0.1 mg/mL) digestion in 37℃. After passing sequentially through 21- and 23- gauge needles, cells were filtered by a 40-µm cell strainer to obtain single-cell suspensions. A mouse lineage cell depletion (order # 130-090-858, Myltenyi Biotech) step was applied according to manufacturer's instruction. The resultant cells were stained for 30 min at 4℃ with PE-CD49f and APC-Sca-1 (eBioscience, San Diego, CA). FACS was performed by using the BD Aria or Fusion (BD Biosciences, San Jose, CA). PI (Propidium iodide) or 7-AAD was added prior to FACS analysis to separate viable from dead cells. As described previously (Valdez et al., 2012), three major populations were defined on the FACS profile as basal ($Sca\text{-}1^+CD49f^{hi}$), luminal ($Sca\text{-}1^-CD49f^{lo}$) and stromal ($Sca\text{-}1^+CD49f^{-/lo}$) cells. For the majority of the experiments, GFP^+ and GFP^- cells were specifically sorted out from the luminal population.

Prostate Tissue Regeneration Assays

Tissue regeneration assays were performed as described (Xin et al., 2003). Briefly, varying number of freshly disassociated prostatic cells or FACS-purified cells were combined with $1.0\sim2.0 \times 10^5$ mouse or rat urogenital sinus mesenchyme (UGM)

in collagen and injected subcutaneously or under the kidney capsule. The outgrowths were harvested for analysis from the experimental mice 2~3 months later.

RNA Isolation and Quantitative RT-PCR (qPCR)

Total RNA was isolated from cells using the RNeasy mini kit (Qiagen, Valencia, CA). The first-strand cDNA synthesis was achieved by reverse transcription of RNA using random hexamers and SuperScript III Reverse Transcriptase (Invitrogen, Grand Island, NY). Quantitative RT-PCR was performed using the iQ™ SYBR® Green supermix (BioRad, Hercules, CA) on a 7900HT Fast Real-Time PCR System (ABI, Applied Biosystems, Foster City, CA). The primers used in this study are listed in Table S3. The housekeeping gene Gapdh or Actb was used as internal control for gene expression normalization.

RNA Sequencing (RNA-seq) and Bioinformatics

For RNA-Seq analysis, freshly purified GFP^+/GFP^- luminal cells were subjected to total RNA extraction using an RNeasy mini kit (Qiagen, Valencia, CA). cDNA libraries were constructed using the TruSeq Stranded Total RNA Preparation Kit (Illumina, cat#: RS-122-2301), which contained Ribo-Zero™ Gold to deplete rRNA. We only amplified our libraries for 10 PCR cycles (instead of 15 suggested by manufacturer) to minimize amplification-induced noise. Purified libraries were quantified using a Kapa library quantification kit (KAPA Biosystems, Wilmington, MA) and then loaded onto a cBot (Illumina, San Diego, CA) at a final concentration of 10 pM to perform cluster generation, followed by 2 x 75 bp sequencing on a HiSeq 2000 (Illumina, San Diego, CA). Two libraries were loaded per lane, yielding an average of 77 M pairs of reads per sample. We mapped the sequencing reads to the reference mouse genome (mm10) using TopHat (version 2.0.10) (Kim et al., 2013) and Bowtie 2 (version 2.1.0) (Langmead and Salzberg, 2012). The number of fragments in each known gene from GENCODE Release M7 (Mudge and Harrow, 2015) was enumerated using htseq-count from HTSeq package (version 0.6.0) (Anders et al., 2015). Genes with fewer than 10 fragments in all samples were removed before differential expression analysis. Differential expression between conditions was statistically assessed by R/Bioconductor package DESeq (version 1.16.0) (Anders and Huber, 2010). Due to the rarity of sorted cells, one sample pooled from multiple sorting was collected for RNA-seq analysis for each cell type. To call differentially expressed genes (DEGs), we used fold change (FC) $\geq$6 and normalized read counts $\geq$20 for bulk luminal GFP^- cells, and FC $\geq$4 and normalized read counts $\geq$10 for rare luminal GFP^+ LRCs. These criteria generated a manageable list of 929 genes preferentially expressed in GFP^+ cells and 1303 genes in GFP^- cells (Table S2).

For Gene Ontology analysis, IPA (Qiagen, Valencia, CA) and DAVID version 6.7 (Huang da et al., 2009) were used with gene symbols. GSEA (the pre-rank function) was carried out by using the curated gene sets (C2) of the Molecular Signature Database (MSigDB) version 4.0 provided by the Broad Institute (http://www.broad.mit.edu/gsea/) (Subramanian et al., 2005). Note that the list of DEGs and entire detectable genes derived from each sample were used for IPA/GO and GSEA analysis, respectively. In particular, we followed the standard procedure as described by GSEA user guide (http://www.broadinstitute.org/gsea/doc/GSEAUserGuideFrame.html). The FDR for GSEA is the estimated probability that a gene set with a given NES (normalized enrichment score) represents a false positive finding, and an FDR <0.25 is statistically significant for GSEA analysis. To reconcile the difference between mouse and human species, the "gene_symbol.chip" function was employed to collapse dataset to gene symbols when performing GSEA. The RNA-Seq data reported in this paper is available in the Gene Expression Omnibus (GEO) database under accession number GSE98760.

Supplemental References

Anders, S., and Huber, W. (2010). Differential expression analysis for sequence count data. Genome biology *11*, R106.
Anders, S., Pyl, P.T., and Huber, W. (2015). HTSeq: a Python framework to work with high-throughput sequencing data. Bioinformatics *31*, 166-169.

Chen, X., Schneider-Broussard, R., Hollowell, D., McArthur, M., Jeter, C.R., Benavides, F., DiGiovanni, J., and Tang, D.G. (2009). Abnormal differentiation, hyperplasia and embryonic/perinatal lethality in BK5-T/t transgenic mice. Differentiation *77*, 324-334.

Huang da, W., Sherman, B.T., and Lempicki, R.A. (2009). Systematic and integrative analysis of large gene lists using DAVID bioinformatics resources. Nat. Protoc. *4*, 44-57.

Jeter, C.R., Badeaux, M., Choy, G., Chandra, D., Patrawala, L., Liu, C., Calhoun-Davis, T., Zaehres, H., Daley, G.Q., and Tang, D.G. (2009). Functional evidence that the self-renewal gene NANOG regulates human tumor development. Stem Cells *27*, 993-1005.

Karthaus, W.R., Iaquinta, P.J., Drost, J., Gracanin, A., van Boxtel, R., Wongvipat, J., Dowling, C.M., Gao, D., Begthel, H., Sachs, N.*, et al.* (2014). Identification of multipotent luminal progenitor cells in human prostate organoid cultures. Cell *159*, 163-175.

Kim, D., Pertea, G., Trapnell, C., Pimentel, H., Kelley, R., and Salzberg, S.L. (2013). TopHat2: accurate alignment of transcriptomes in the presence of insertions, deletions and gene fusions. Genome Biol. *14*, R36.

Langmead, B., and Salzberg, S.L. (2012). Fast gapped-read alignment with Bowtie 2. Nature methods *9*, 357-359.
Liu, C., Kelnar, K., Liu, B., Chen, X., Calhoun-Davis, T., Li, H., Patrawala, L., Yan, H., Jeter, C., Honorio, S.*, et al.* (2011). The microRNA miR-34a inhibits prostate cancer stem cells and metastasis by directly repressing CD44. Nat. Med. *17*, 211-215.

Mudge, J.M., and Harrow, J. (2015). Creating reference gene annotation for the mouse C57BL6/J genome assembly. Mamm. Genome *26*, 366-378.

Subramanian, A., Tamayo, P., Mootha, V.K., Mukherjee, S., Ebert, B.L., Gillette, M.A., Paulovich, A., Pomeroy, S.L., Golub, T.R., Lander, E.S.*, et al.* (2005). Gene set enrichment analysis: a knowledge-based approach for interpreting genome-wide expression profiles. Proc. Natl. Acad. Sci. USA *102*, 15545-15550.

Tumbar, T., Guasch, G., Greco, V., Blanpain, C., Lowry, W.E., Rendl, M., and Fuchs, E. (2004). Defining the epithelial stem cell niche in skin. Science *303*, 359-363.

Valdez, J.M., Zhang, L., Su, Q., Dakhova, O., Zhang, Y., Shahi, P., Spencer, D.M., Creighton, C.J., Ittmann, M.M., and Xin, L. (2012). Notch and TGFbeta form a reciprocal positive regulatory loop that suppresses murine prostate basal stem/progenitor cell activity. Cell Stem Cell *11*, 676-688.

Xin, L., Ide, H., Kim, Y., Dubey, P., and Witte, O.N. (2003). In vivo regeneration of murine prostate from dissociated cell populations of postnatal epithelia and urogenital sinus mesenchyme. Proc. Natl. Acad. Sci. USA *100 Suppl 1*, 11896-11903.

Zhang, D., Jiang, P., Xu, Q., and Zhang, X. (2011). Arginine and glutamate-rich 1 (ARGLU1) interacts with mediator subunit 1 (MED1) and is required for estrogen receptor-mediated gene transcription and breast cancer cell growth. J. Biol. Chem. *286*, 17746-17754.